



Article

# SARS-CoV-2 S Mutations: A Lesson from the Viral World to Understand How Human Furin Works

Leonardo Cassari <sup>1,†</sup> , Angela Pavan <sup>2,†</sup> , Giulia Zoia <sup>2</sup>, Monica Chinellato <sup>2</sup>, Elena Zeni <sup>1</sup>,  
Alessandro Grinzato <sup>3</sup> , Sylvia Rothenberger <sup>4,5</sup> , Laura Cendron <sup>2</sup> , Monica Dettin <sup>1</sup>   
and Antonella Pasquato <sup>1,\*</sup>

<sup>1</sup> Department of Industrial Engineering, University of Padova, Via Marzolo 9, 35131 Padova, Italy

<sup>2</sup> Department of Biology, University of Padua, Viale G. Colombo 3, 35131 Padova, Italy

<sup>3</sup> European Synchrotron Radiation Facility, 71, Avenue des Martyrs, 38000 Grenoble, France

<sup>4</sup> Institute of Microbiology, University Hospital Center and University of Lausanne, Rue du Bugnon 48, 1011 Lausanne, Switzerland

<sup>5</sup> Spiez Laboratory, Federal Office for Civil Protection, Austrasse, 3700 Spiez, Switzerland

\* Correspondence: antonella.pasquato@unipd.it

† These authors contributed equally to this work.

**Abstract:** Severe acute respiratory syndrome coronavirus-2 (SARS-CoV-2) is the etiological agent responsible for the worldwide pandemic and has now claimed millions of lives. The virus combines several unusual characteristics and an extraordinary ability to spread among humans. In particular, the dependence of the maturation of the envelope glycoprotein S from Furin enables the invasion and replication of the virus virtually within the entire body, since this cellular protease is ubiquitously expressed. Here, we analyzed the naturally occurring variation of the amino acids sequence around the cleavage site of S. We found that the virus grossly mutates preferentially at P positions, resulting in single residue replacements that associate with gain-of-function phenotypes in specific conditions. Interestingly, some combinations of amino acids are absent, despite the evidence supporting some cleavability of the respective synthetic surrogates. In any case, the polybasic signature is maintained and, as a consequence, Furin dependence is preserved. Thus, no escape variants to Furin are observed in the population. Overall, the SARS-CoV-2 system per se represents an outstanding example of the evolution of substrate–enzyme interaction, demonstrating a fast-tracked optimization of a protein stretch towards the Furin catalytic pocket. Ultimately, these data disclose important information for the development of drugs targeting Furin and Furin-dependent pathogens.

**Keywords:** Furin; protease; SARS-CoV-2; cleavage; peptide; in vitro; glycoprotein S; envelope glycoprotein; virus



**Citation:** Cassari, L.; Pavan, A.; Zoia, G.; Chinellato, M.; Zeni, E.; Grinzato, A.; Rothenberger, S.; Cendron, L.; Dettin, M.; Pasquato, A. SARS-CoV-2 S Mutations: A Lesson from the Viral World to Understand How Human Furin Works. *Int. J. Mol. Sci.* **2023**, *24*, 4791. <https://doi.org/10.3390/ijms24054791>

Academic Editor: James K. Bashkin

Received: 30 January 2023

Revised: 17 February 2023

Accepted: 20 February 2023

Published: 1 March 2023



**Copyright:** © 2023 by the authors. Licensee MDPI, Basel, Switzerland. This article is an open access article distributed under the terms and conditions of the Creative Commons Attribution (CC BY) license (<https://creativecommons.org/licenses/by/4.0/>).

## 1. Introduction

December 2019 went down in history as the month when a new deadly virus was first identified. The initial spread flew under the radar until a significant number of cases of atypical pneumonia suddenly caught people's eye. At that point, the entire planet witnessed the astonishing measures taken to curb the contagion across the population within the city of Wuhan, Hubei Province, Central China, which was the first site of the viral outbreak. Unfortunately, the attempts failed to limit the infection that quickly spread worldwide. As of September 2022, 600 million confirmed cases and 6.5 million deaths had been reported by the World Health Organization (WHO) (<https://covid19.who.int/>). The virus responsible for the pandemic was identified as a novel member of the *Coronaviridae* family and named as severe acute respiratory syndrome coronavirus-2 (SARS-CoV-2). The WHO called the disease associated with SARS-CoV-2 coronavirus disease-19 (COVID-19), and it was the virus first reported in the year 2019 [1].

SARS-CoV-2 is thought to have emerged from bats, possibly via a secondary host [2]. Several factors have been crucial for the global human pandemic, including—but not limited to—the acquisition of specific mutations that allowed binding to the human receptor [3] and the insertion of key amino acids that made the virus maturation dependent on human ubiquitous proteases [4]. Multiple other aspects need to be taken into consideration and have contributed to the spread and the severity of the viral infection of SARS-CoV-2. For example, age of population, concomitant diseases [5], and variations in human lifestyle (such as diet), along with microbiota, which play a crucial role in health and immunity against viral infections [6,7]. Since the very first infection and human-to-human propagation, SARS-CoV-2 has rapidly co-evolved with its host. In the initial stages of the pandemic, viral evolution was shaped by selection imposed by a naïve host and the environment, resulting in new variants with adaptive advantages rapidly taking over previous strains. The scenario changed following the advent of vaccines, resulting in the increase in immune-evading variants [8–11].

SARS-CoV-2, as with all viruses, is an opportunistic agent, which relies on the infected host for its replication and dissemination. Since the very first contact with the target cell, and the delivery of its genetic material and thereafter full cell colonization, SARS-CoV-2 manipulates and re-programs the host to its advantage [12]. A key step of the virus life-cycle is the synthesis and maturation of the protein spike S, which sits on the surface of budding particles [13]. Only S-decorated virions are competent for cellular receptor(s) engagement and membrane fusion [14]. The glycoprotein S is made of 1273 amino acids, is membrane anchored, and heavily undergoes glycosylation and further cleavage, leading to the mature heterodimer S1/S2. The entire synthesis and post-translation modifications occur at the expense of the cellular machinery, which provide a de facto for all the virus needs to generate a new progeny of infectious virions. Most importantly, the processing of the glycoprotein occurs at the  ${}_{682}\text{RRAR}_{685}\downarrow$  motif and it is mediated by Furin (Figure 1) [15–17]. The maturation of S into S1/S2 is crucial for infectivity [15], thus processing represents a major drug target to contain infection [18]. Furin is a member of the basic Proprotein Convertases (PCs) family, whose distinctive mark is the ability of cutting protein substrates after polybasic clusters, typically  $\text{BX}_n\text{R}\downarrow$  where B is a basic residue, X is any amino acid except Cys, and n is 0,2,4,6,8 [19]. Proteolytic activation by Furin is likely an important feature that allowed SARS-CoV-2 to overcome the species barriers and thus cause human disease [20]. In the human body, Furin is ubiquitously expressed. Accordingly, any organ becomes a platform for the release of infectious particles, explaining the highly lethal nature and high rate of multiple-system failure caused by SARS-CoV-2 colonization [21]. In contrast, protease cleaving after single basic residues (e.g., airway trypsin-like protease HAT) is typically restricted to specific body parts, such as the upper respiratory tract or intestine [22]. Thus, pathogens depending upon this class of enzymes show more restricted host invasion [23].

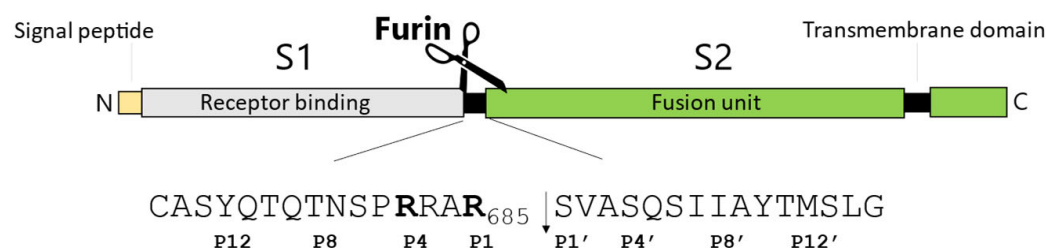


**Figure 1.** Schematic representation of the envelope glycoprotein S of SARS-CoV-2 and its cleavage site (sequence 671–700). Amino acids, one-letter code. Key arginines for Furin recognition are in bold. The scissile bond is designated by an arrow. Positions upstream (P12 to P1) and downstream of the cleavage (P1' to P12') are specified.

The Furin cleavage site (FCS) of the envelope glycoprotein S is the result of a 12-nucleotide insertion encoding for an extra  ${}_{681}\text{PRRA}_{684}$  motif, switching the solitary

arginine R↓ into the polybasic cluster PRRAR↓ [24,25]. This special insertion rendered the glycoprotein sensitive to Furin, nodding to the speculations that the virus may be artificial. Indeed, SARS-CoV-2 S processing is exceptional when compared to other SARS-related coronaviruses. However, sequence analysis has shown that the natural evolution of the S glycoprotein is highly probable [26,27]. A direct consequence of the insertion is the easier maturation of the SARS-CoV-2 spike, which is processed to higher efficiency rates compared to the cognate glycoprotein of the SARS-CoV [28]. The extra PRRA motif was a random event that generated a minimal Furin consensus site within the S polypeptide that started to acquire further mutations as a consequence of the interaction with the enzyme. Due to the large number of infected people worldwide, several variants carrying single or multiple amino acid replacements around the FCS have been reported. Public health agencies—such as the World Health Organization—have assigned some mutants as variants of concern (VOCs). Over the course of the pandemic, two of these VOCs (B.1.1.7 [Alpha] and B.1.617.2 [Delta]) have independently risen to prominence, rapidly replacing the previously circulating strains [29]. The FCS spike from the Alpha and Delta lineages show P681R and P681H replacements, respectively. Most recently, a new isolate has been taking over, namely the Omicron variant. The latter harbors multiple spike mutations, two of which—N679K and P681H—sit close to the Furin scissile bond [30].

Several studies have disclosed that the presence of a Furin cleavage site at the S1/S2 boundary confers additional advantages to the virus, which acquires an increased fitness in terms of an overall enhanced ability to infect [15,31–33]. The gain-of-function (GOF) phenotype relies on the ability of the virus to exploit the polybasic cluster for further activities besides using it to mature the envelope glycoprotein. As time goes on, various functions have been gradually discovered, shedding some light on a complex scenario in which RRAR<sub>685</sub>↓ turns out to have prominent roles within the whole virus life-cycle. At the entry level, FCS was found to be a key factor for receptor binding by grossly favoring virus attachment to the main cellular receptor, the angiotensin-converting enzyme 2 (ACE2) [34]. Moreover, FCS broadens the receptor options by mediating the interaction between the envelope glycoprotein S and neuropilin-1 (NRP1) [35] or Heparan Sulfate (HS) [36,37]. NRP1 and HS recognize the C-term Arg and XBBXB binding motif, respectively, present within the viral <sub>680</sub>SPRRARS<sub>686</sub> stretch. The FCS was further shown to be required for the following steps of fusion, syncytium formation [15,38] and human cell invasion [39]. Furthermore, the Furin cleavage reduces SARS-CoV-2 sensitivity to innate immune restriction, mediating an early escape from the IFN-induced transmembrane (IFITM) sensors [31]. Vice versa, synthetic variants lacking the polybasic motifs were shown to possess attenuated virulence. Accordingly, despite the appearance of multiple different variants worldwide, natural FCS deletion mutants—e.g.,  $\Delta_{680}$ SPRRA<sub>684</sub> and  $\Delta_{685}$ RSVA<sub>688</sub>—are extremely rare events, suggesting that the cleavage site is under strong selective pressure in humans [40]. Of note, the removal of the entire <sub>679</sub>NSPRRAR<sub>685</sub> stretch may easily arise when the virus is cultured in vitro [41]. Along these lines, SARS-CoV-2 was shown to rapidly adapt upon culture Vero E6 cells, due to increased cleavage efficiency by cathepsins at the mutated S cleavage site [39]. That is, S1/S2 switching to other proteases is possible, although this option is restricted in vivo, suggesting that there is a tight virus–enzyme interconnection through a mechanism(s) that has yet to be discovered. Finally, it is noteworthy that Furin masters a plethora of functions in virtually all organs. It is conceivable that the massive production of viral spikes competes with endogenous substrates, leading to enzyme dysregulations to further favor viral infection. An example is offered by the sodium epithelium channels (ENaCs), protein complexes critical for the homeostasis of airway surface liquid, whose misregulation is associated with adverse respiratory conditions. ENaC is activated by Furin but undergoes alterations when the envelope glycoprotein S of SARS-CoV-2 is expressed [42].

Understanding the impact of cleavage-site mutations on spike cleavability is important for fighting against SARS-CoV-2 and designing new antivirals. Whether a single amino acid replacement enhances maturation may explain why some viral strains are widespread.

Additionally, it may provide evidence that we should be on the alert for forthcoming variants outbreaks. In parallel, new residues at the cleavage site may provide new targetable interactions to develop potent drugs. Importantly, the most-spread variants represent unique events to best pinpoint Furin substrates. The enforced co-existence between SARS-CoV-2 and Furin and the intrinsic virus propensity to mutation resulted de facto in a large in vivo library screening. Indeed, a huge number of combinations of amino acids around the cleavage site has entered into contact with the enzyme, with those with enhanced viral fitness being more successful.

In this study, we focused on the Furin cleavage site of the SARS-CoV-2 glycoprotein S by exploring the GISAID sequences database and reproducing in vitro the most significant mutations to understand the mechanism(s) of adaptation of the pathogen to the human Furin protease. More in detail, we analyzed the SARS-CoV-2 spike sequences of circulating strains and found that major mutations occur upstream of the cleavage site, whereas RRAR<sub>685</sub>↓ is highly conserved. In particular, P681 is either replaced by Arg (Delta variant) or His (Beta/ Omicron variant), but not Lys, despite our studies on synthetic substrates suggesting that it may represent a suitable alternative. Distant variants—Q675H, Q677H and T678I—confer an increased cleavability to 17mer substrates mimicking the cleavage site. Of note, the presence of a histidine is a mark for a broader pH optimum. Peptide conformational investigations exclude major structural differences among mutants. Thus, the increased cleavability points the finger towards an improved substrate–enzyme interaction. Taken together, our findings refine our current knowledge on Furin substrate specificity. In particular, we now understand the importance of the amino acids neighboring the minimal cleavage site RXXR↓.

## 2. Results

### 2.1. SARS-CoV-2 Spike S Varies Close to the Furin Cleavage Site Preferentially at P Positions

The way a substrate is recognized by Furin is not symmetrical since six amino acids before and only two after the scissile bond—P6-P2' positions—match the catalytic pocket [43,44]. While scientists agree that polybasic amino acids are a “must” at P positions, little is known on the preference of Furin within the P' stretch. The MERPOS database (<https://www.ebi.ac.uk/merops/index.shtml>, accessed on 1 March 2022) shows that Ser and Val are favored at P1' and P2', respectively, within a library of 90 officially recognized Furin substrates. Flanking residues, both upstream of the P6 and downstream of the P2' positions, can still be important in terms of making the core available to the enzyme [45]. Thus, the latter can modulate the kinetics of cleavage, rendering a protein a superior or lousy substrate.

Based on these premises, at the level of the SARS-CoV-2 spike maturation site, we expected little or no variations of the key Arg at P1 and P4, as well as Ser and Val at P1' and P2', respectively. In contrast, we anticipated variations of the surrounding residues to be more likely. The SARS-CoV-2 glycoprotein S contains a unique extra “PRRA” motif at the S1/S2 boundary (P2-P5 positions) that is not present in the other coronaviruses such as SARS-CoV-1 and MERS-CoV [24,46] (Figure 1).

The “appearance” of this polybasic cluster changed the consensus motif of the envelope glycoprotein, and the coronavirus became Furin-dependent, in spite of a non-ideal distribution of amino acids all around it. It is conceivable that during the massive viral spread among the human population, the selected random mutations occurring within the spike glycoprotein may be associated to an enhancement of cleavage by the Furin enzyme [47]. To verify this hypothesis, we first performed virtual amino acid scanning by replacing each residue within the 671-700 region (P15-P15') of S wild-type (Reference sequence <sub>671</sub>CASYQTQTNSPRRAR↓SVASQSIIAYTMSLG<sub>700</sub>; isolate Wuhan-Hu-1; GenBank: MN908947.3) with the other 19 available alternatives and searched for actual variants based on the sequences deposited in the GISAID database (<https://outbreak.info/situation-reports>, 30 August 2022) [48] (Figure 2 and Table S1). More in detail, we searched for the existence of SARS-CoV-2 spike variants carrying one single

mutation at a time. All possible combinations were explored, e.g., C671 was replaced by any residue among R, K, H, D, E, Q, N, T, S, F, Y, W, P, I, L, V, G, A, and M. Along the same lines, all amino acids surrounding the cleavage site (P15-P15') underwent a similar analysis. The number of glycoprotein sequences carrying a specific mutation and deposited in the database was annotated accordingly (Table S1) and graphically represented in a 3D plot. Graph spikes highlight major mutations that occurred and the occurrence of each one of them (Figure 2). The analysis was performed on 30 August 2022.

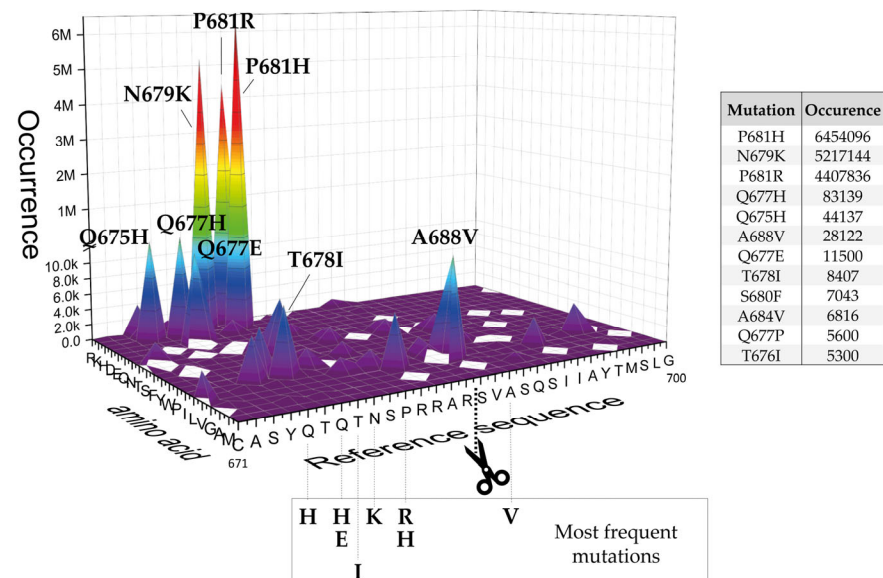


**Figure 2.** Occurrence of mutants within the SARS-CoV-2 S cleavage site  ${}_{671}\text{CASYQTQTNSPRRRARSVASQSIIAYTMSL}_{700}$  (GISAID sequence database).

Overall, we found that residues at P positions vary much more than those at P' positions, in line with the evidence that the Furin catalytic site preferentially recognizes stretches before the scissile bond rather than after. Thus, the refinement of the trait upstream of the cleavage overtakes that of the downstream part. More in detail:

1. The replacement of the key R685 and R682 at P4 and P1, as well as S686 at P1', is a rare event (1108, 627, and 193 over 12.335.229 total sequences, respectively), as expected. Interestingly, we performed a similar database analysis on 10 January 2022, thus excluding the SARS-CoV-2 sequences uploaded in the GISAID platform from 11 January to 30 August 2022. Comparing the two analyses, we found that mutations at R682 are recent acquisitions. Indeed, more than 90% of the actual variants have been reported this year (52 vs. 575 from 11 January to 30 August 2022);
2. The most popular variations occur at odd positions (P5, P7, P9, and P11) by replacing WT residues with basic amino acids. Of note, the closer the position is to the cleavage bond, the higher the number of recorded variants. Position P1, cleavage site, R<sub>685</sub>↓ Position P5, P681H + P681R —10.861.932 mutants Position P7, N679K ——— 5.217.144 mutants Position P9, Q677H ——— 83.139 mutants Position P11, Q675H ——— 44.137 mutants
3. The variation of residues at even-numbered positions (P6, P8, and P10) is much less frequent. Here, mutations involve the accommodation of amino acids with a hydrophobic character;
4. Finally, there is nothing noteworthy within the P' region, except the conservative A688V mutation at P3'.

Grouping the mutants by position, we observed a clear cluster of hydrophilic variants increasing around the region before the cleavage site, whereas an opposite trend was found for the stretch following the scissile bond. Interestingly, some classes of amino acids are under-represented, such as the acidic D and E (Figure 3).

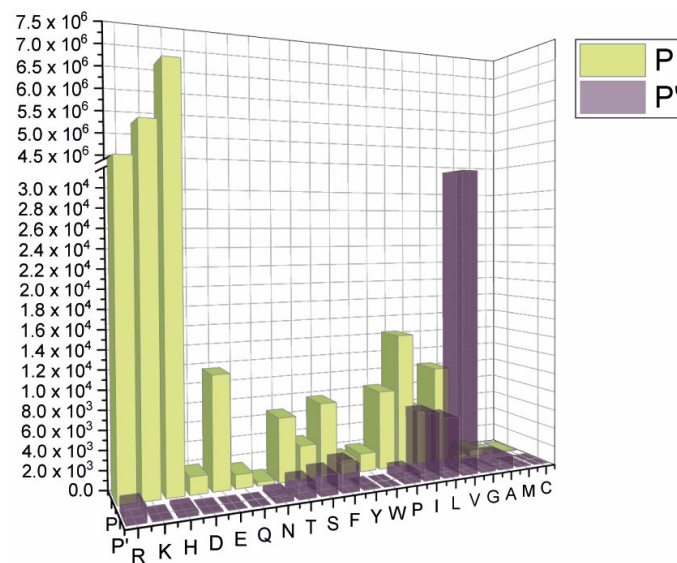


**Figure 3.** Prevalence of amino acid mutations based on either P (before cleavage) or P' (after cleavage) positions within the SARS-CoV-2 S cleavage site  $_{670}$ CASYQTQTNSPRRARSVASQSIIAYTMSL $_{700}$  (GISAID sequence database).

Eventually, for each position within the P15-P15' area, we scored the most frequent amino acid replacements, taking them individually (Figure 4).

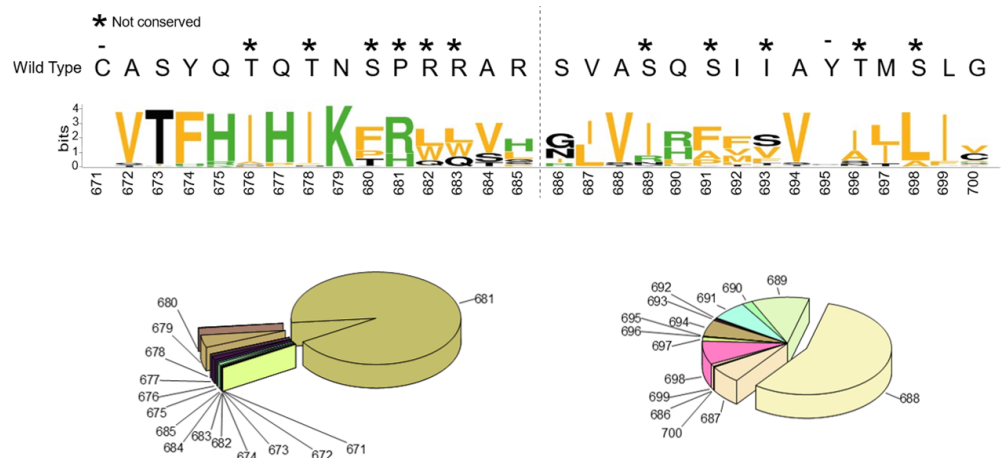


**Figure 4.** (Top) Sequence logo relative to the spike SARS-CoV-2 S shows the most popular naturally occurring amino acid replacement for each position, taken individually (<https://weblogo.berkeley.edu/logo.cgi>, 30 August 2022); (Bottom) Statistic cake images reporting the relative contribution of the sum of all mutant sequences at a given position, grouped according to P (left) and (P') residues.

C671 was no match for any other amino acid, underlying its prominent function. In fact, Cys at 671 is engaged in a disulfide bridge with Cys 662 and it is crucial for the overall architecture of the spike protein [49]. Similarly, Tyr 695 is also invariable, probably due to the very favorable T-shaped  $\pi$  stacking interaction established with the side chain of the aromatic Tyr 660, stabilizing the protein structure. Actually, Tyr 695 and Tyr 660, together with Ile 693 and Val 656, form a singular highly hydrophobic pocket (Figure 5).

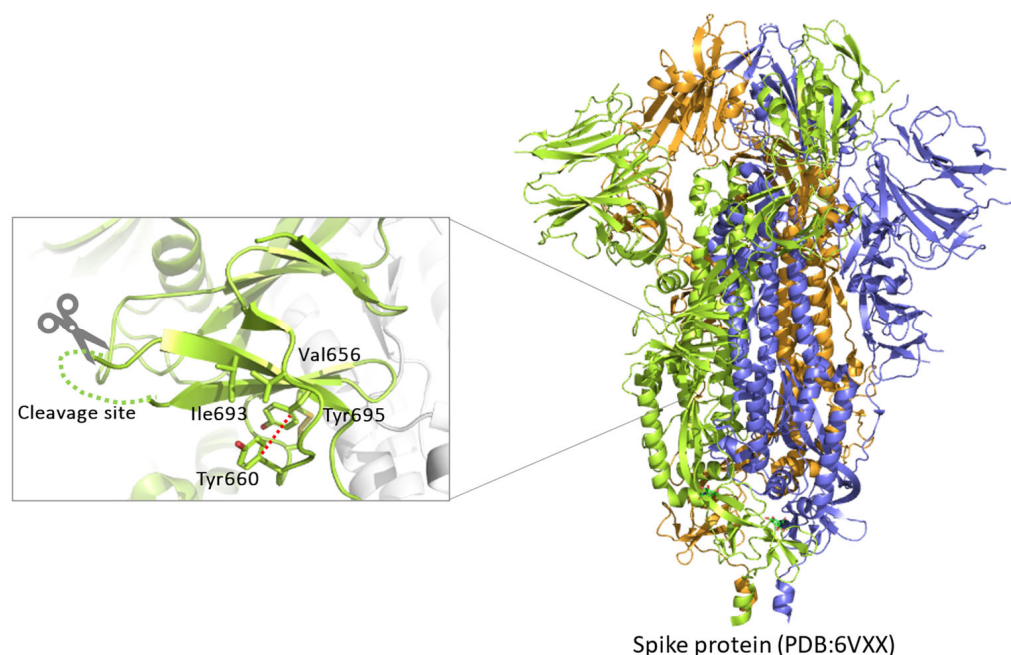


**Figure 5.** Cartoon view of spike glycoprotein trimers in closed conformation (right panel, PDB 6VXX). Zoomed view (left panel) of one of the cleavage sites: side chains (sticks view) of residues forming an adjacent hydrophobic cleft are evidenced, and the stacking interaction is traced (red dashed line).

The P14-P11 tetrapeptide accommodates conserved replacements: hydrophobic with hydrophobic, aromatic with aromatic, and hydrophilic with hydrophilic. P10-P11 are promiscuous. Interestingly, the P9-P3 stretch—harboring the PRR motif—has the propensity to switch its physical chemical properties. That is, the amino acids corresponding to the insertion have the tendency to acquire a different identity when compared to the original circulating strain. Of note, we observed the rise of Trp-containing variants, though this happens in a limited number of sequences. Tryptophan possesses a bulky aromatic side chain and therefore it may impose local structural constraints to the substrate, right into the catalytic pocket. With regards to the P1'-P15' positions, the majority varies in a conservative fashion (Figure 4). Overall, we verified that the key residues required for recognition by the Furin enzyme are tightly preserved. Variations of the S1/S2 boundary occur preferentially at P positions, with the appearance of selected amino acids at odd-numbered positions.

## 2.2. *In Vitro* Digestion of Peptides Mimicking the Cleavage Site of SARS-CoV-2 Spike Variants

### 2.2.1. Neutral pH Privileges Cleavage of SARS-CoV-2 S WT

The Furin enzyme has a pH optimum of around 7.0, with more than 50% of its enzymatic activity between pH 5 and 8, depending on the substrate being cleaved [50,51]. The broad pH spectrum reflects the ability of Furin to work in different subcellular compartments, including Golgi, endosomes, and plasma membranes [52], each of these having unique  $[H^+]$  contents. Indeed, in eukaryotic cells, the steady-state pH of intracellular compartments varies greatly. Typically, organelles along the secretory pathway are characterized by progressive acidification, from the pH 7.2 of Endoplasmic Reticulum to the pH ~6 of late Golgi stacks [53]. Most envelope glycoproteins of Furin-dependent viruses are cleaved in their way out through the secretory pathway, prior to reaching the viral budding platforms. This is the case of influenza [54], paramyxo [55], retro [56], and hemorrhagic fever [57] viruses, among others. Similarly, SARS-CoV-2 S was found to be cleaved by Furin in the TGN [17]. To investigate the cleavability of SARS-CoV-2 S by Furin in different pH conditions, we transiently expressed the viral glycoprotein lacking the transmembrane domain and the C-term His tag [4] in HEK293 cells. Supernatants were collected at 72 h post transfection (p.t.) and purified by ion-exchange chromatography. Of note, the purified protein contained a fraction of cleaved S, the latter generated by endogenous Furin. Digestions

were carried out at 37 °C with soluble human Furin (sFur) [58] at pH, 5.5, 7.0, and 8.0 (25 mM sodium acetate pH 5.5 or 25 mM HEPES (4-(2-hydroxyethyl)-1-piperazineethanesulfonic acid) pH 7.0, supplemented with 2mM CaCl<sub>2</sub>). Relative sFur activity was validated on the Pyr-RTKR-AMC substrate and Furin-specific inhibitor Dec-RVKR-chloromethylketone (Figure S1). Samples were collected at 1, 4, and 7 h and O/N. For each time point, the cleavage reaction was promptly stopped by adding EDTA 0.5M prior to boiling at 95 °C for 5 min. All samples were then stored at −80 °C until final analysis by Western blotting (WB). We found that all three pH levels tested (5.5, 7.0, and 8.0) were suitable for inducing—although differently—full protein processing (the disappearance of S O/N). Accordingly, basic and neutral conditions were more favorable, in particular at early time points (Figure 6a). Interestingly, the conversion of S to S1/S2 was very fast upon the addition of the enzyme (compare control vs. t<sub>0</sub>, (Figure 6a)) and slowed down thereafter, possibly underlying some regulatory mechanisms of Furin activity when products are generated. We repeated an analogous experiment using the synthetic <sup>673</sup>SYQTQTNSPRRAR↓SVAS<sub>689</sub> stretch as a substrate. The sequence encompasses the cleavage site (P13-P4') of the envelope glycoprotein S. Briefly, the 17mer peptides were chemically synthesized (Solid Peptide Phase Synthesis (SPPS), Fmoc-chemistry), purified and characterized following standard protocols. The peptide was incubated at 5 μM with recombinant soluble human Furin in suitable buffer (pH 5.5, 7.0, and 8.0) at 37 °C. Digestions were performed as independent triplicates. Samples were collected at regular intervals over 6 h and processed as described above, with the final analysis including reverse phase (RP) high-performance liquid chromatography (HPLC) coupled with ultraviolet (UV) detection (214 nm) to visualize the area corresponding to the unprocessed peptide (Figure S2). Areas relative to the intact peptide were calculated and plotted over time to visualize the disappearance of the substrate following cleavage by Furin. Cleavage at R685 was confirmed by mass spectrometry analysis (Figure S3). In these settings, pH 7.0 was by far the most efficient condition to promote cleavage (Figure 6b and Figure S2).

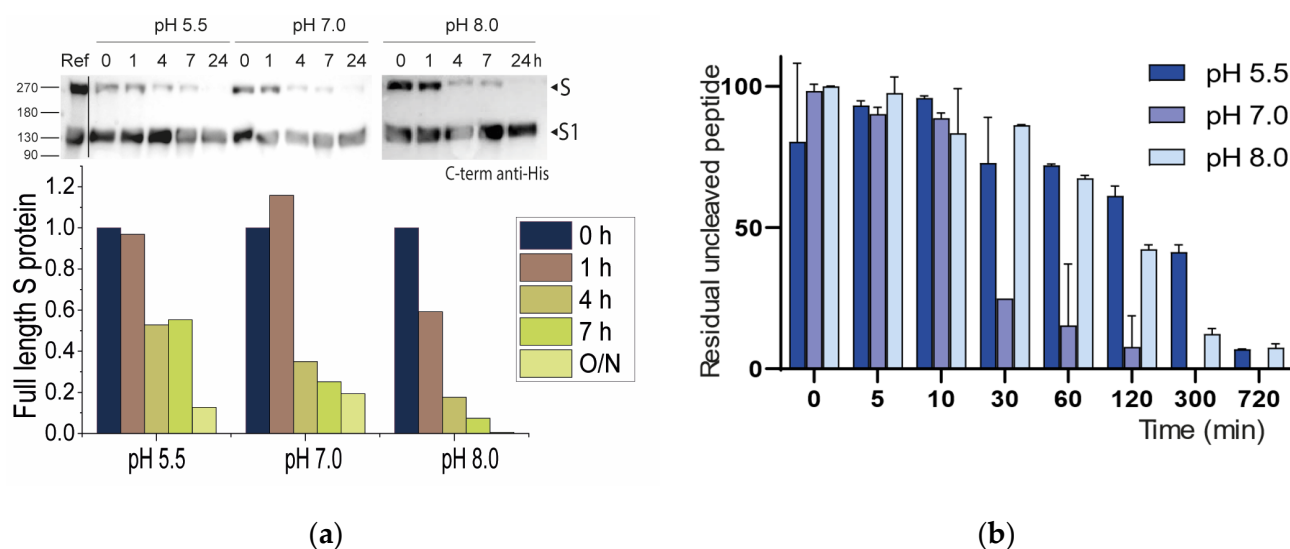


**Figure 6.** (a) Western blot analyses of SARS-CoV-2 glycoprotein cleaved at different pH levels. Bands correspond to the FL protein that disappears upon incubation with sFur over time. Control, FL spike, without the addition of sFur. O/N, overnight. Anti-His antibody was used to detect the protein; (b) In vitro cleavage of <sup>673</sup>SYQTQTNSPRRAR↓SVAS<sub>689</sub>. The peptide was incubated with sFur as described in the Materials and Methods section. Extension of cleavage was evaluated as residual uncleaved peptide detectable by HPLC at 214 nm. Areas under the peak of the uncleaved peptide at time 0 min were arbitrarily taken as reference. Experiments were performed as triplicates.

Overall, the data are compatible with a processing event occurring in the Golgi, as previously reported [17]. In this compartment, the SARS-CoV-2 glycoprotein passes

through to meet the TGN-resident Furin enzyme prior to reaching the plasma membrane. For the peptide, the processing pH optimum is centered around neutral values, although this is less striking when considering the entire S molecule. Possibly, regions outside the cleavage site are able to influence the interaction between the protease and its substrates. This finding is consistent with other reports where single-point mutations close to the scissile bond were found to impact cleavage differently, either according to the actual S backbone where they are inserted and/or based on the substrate length. Kinetics further suggest that early times are crucial to generate the mature forms.

### 2.2.2. Histidines Upstream of the Cleavage Site Result in Gain-of-Function (GOF) Variants

Histidines are the most represented residues across all mutations (Figure 2). These are “special” amino acids, being protonated in a slightly acidic environment or bearing no charge at  $\text{pH} \geq 7$ . Indeed, at low pH, both  $\delta$ -nitrogen and  $\epsilon$ -nitrogen of the imidazole ring of the side chain are protonated and the amino acid shows an overall +1 charge. At high pH, the histidine is neutral, with neither  $\delta$ -nitrogen nor  $\epsilon$ -nitrogen being protonated. Due to their bivalence, histidines are known to be master regulators of several biological functions. The rate of conversion of a given substrate into its cleaved products is no exception, e.g., the PrM of Dengue virus contains a key H68 close to the processing site, which is crucial for maturation [49]. Therefore, it is conceivable that the consistent appearance of SARS-CoV-2 variants carrying His residues around the cleavage site of the glycoprotein S is an indication of the adaptation of the virus to the host, in order to better exploit the Furin protease at broader pH conditions. This can be achieved by increasing the substrate/catalytic pocket affinity and/or by the adoption of a more favorable conformation so that the cleavage stretch may dock the enzyme easier. To understand the impact of histidines on the processing event, we approached the question by studying the cleavability of synthetic 17mer peptides encompassing the SARS-CoV-2 spike (P14-P4') region (Table 1). We focused our attention on P681H (Alpha), Q677H, Q675H and the recently identified N679K/P681H (Omicron) variants.

P681H was first identified in the UK in late 2020 [59] and then classified as the VOC variant “Alpha” [60]. It was proposed to increase the accessibility of the cleavage site, leading to enhanced processing by a mechanism that relies on the loss of a nearby O-glycosylation that is P681 dependent [27]. The same mutation may also impact the local conformation and thus further favor the binding affinity of the S protein to Furin [61]. The increase of S maturation into S1/S2 is controversial [62–64]. Very recently, a fluorogenic 11mer peptide (P8-P3') carrying P681H was shown to be digested similarly to the analogous WT peptide at pH 7.5 and poorly in acidic conditions [64]. Q675H mutation arose independently in separate evolutionary clades in early pandemic times, and it was suggested to favor processing by conferring a lower structural variability to the Furin cleavage-site loop [65]. Q677H also emerged early in multiple lineages of the SARS-CoV-2 spike protein [66]. Both Q675H and Q677H are VOCs and have been linked to an increased SARS-CoV-2 fitness [67]. Finally, the N679K/P681H Omicron variant is the currently circulating strain, detected for the first time at the end of 2021 and carrying an unusual cluster of mutations, especially within the envelope glycoprotein [68]. Intriguingly, while the full-length S was shown to be cleaved less efficiently than the WT [69], the fluorogenic peptide  ${}_{678}\text{TKSHRRAR}\downarrow\text{SVA}_{688}$  was shown to be a superior Furin substrate [70]. The digestions and analyses of our 17mer peptides were carried out as described above, monitoring the cleavage extent after 1 hr of incubation at 37 °C. Data were corrected for HPLC injection, taking as reference an invariable impurity detected at ~ 21 min (Figure S4). Due to the sensitivity of histidine to acidic conditions, reactions were performed at pH 5.5, 6.5 and 7.0. We observed that all peptides were cleaved better than the WT in acidic conditions (Figure 7a–d,g). Of note, digestions at pH 5.5 seem to occur very quickly, with the precursor at  $t_0$  already being partially cleaved. Therefore, peptides appear to perform similarly to the full-length S that drastically decreased upon Furin addition (Figure 6a). The Omicron peptide carrying the double N679K/P681H mutation is a superior

Furin substrate at all pH values tested, in line with previous reports [70]. Q677H is the worse replacement, being the corresponding peptide poorly digested at neutral pH and to some extent at pH 5.5. Interestingly, the latter shows a profile similar to that found for the P681R peptide (Figure 7f), which mimics the cleavage site of the Delta variant, one of the very early widespread mutants [71]. The poor cleavability of the P681R peptide was quite unexpected since very short sequences from Delta SARS-CoV-2 are reported to be GOF variants [72]. Discrepancies may be due to the different lengths of the peptides used in this work. Moreover, unlike [72], we strictly opted for natural amino acids without the use of additional groups that may favor cleavage readout (e.g., fluorescent groups) but—at the same time—may alter kinetics. In line with these thoughts, it was suggested that P681R contributes to an increased spike cleavability, although this mutation is not fully responsible [62]. Further, Zhang and colleagues showed that P681R affects full-length spike processing by modulating its glycosylation. Thus, the abrogation of specific glycosylation pathways makes P681R irrelevant to the cleavage extent [73].

**Table 1.** Sequences (one-letter code for all amino acids except ornithine, which is indicated by Orn) In yellow, mutations vs. wild-type. Theoretical mass refers to the calculated monoisotopic molecular weight; Experimental mass refers to the molecular weight found by MALDI-Mass Spectrometry analyses.

	ID	P13	P12	P11	P10	P9	P8	P7	P6	P5	P4	P3	P2	P1	P0	Theoretical Mass [Da]	Experimental Mass [Da]			
Synthetic: Naturally occurring	Wild Type (WT)	S	Y	Q	T	Q	T	N	S	P	R	R	A	R	S	V	A	S	1908.05	1907.61
	Q675H	S	Y	H	T	Q	T	N	S	P	R	R	A	R	S	V	A	S	1917.06	1917.69
	Q677H	S	Y	Q	T	H	T	N	S	P	R	R	A	R	S	V	A	S	1917.06	1917.52
	T678I	S	Y	Q	T	Q	I	N	S	P	R	R	A	R	S	V	A	S	1920.11	1920.63
	N679K, P681H	S	Y	Q	T	Q	T	K	S	H	R	R	A	R	S	V	A	S	1962.15	1962.46
	P681H	S	Y	Q	T	Q	T	N	S	H	R	R	A	R	S	V	A	S	1948.08	1948.55
	P681R	S	Y	Q	T	Q	T	N	S	R	R	R	A	R	S	V	A	S	1967.12	1968.61
	P681K	S	Y	Q	T	Q	T	N	S	K	R	R	A	R	S	V	A	S	1939.11	1939.87
	P681Orn	S	Y	Q	T	Q	T	N	S	Orn	R	R	A	R	S	V	A	S	1925.07	1925.65
		amino acid position	673	674	675	676	677	678	679	680	681	682	683	684	685	686	687	688	689	

In summary, the replacement of WT residues with histidines near the scissile bond renders the peptide more cleavable in acidic conditions. Thus, P681H, Q675H and N679K/P681H overcome the WT peptide processing outcome. The ability of single mutations beyond the minimal RRAR<sub>685</sub>↓ motif to modulate Furin activity is astonishing in these examples. Targeting this peripheral region may be a preferential approach to blocking glycoprotein maturation, as an alternative to directly attacking the polybasic motif.

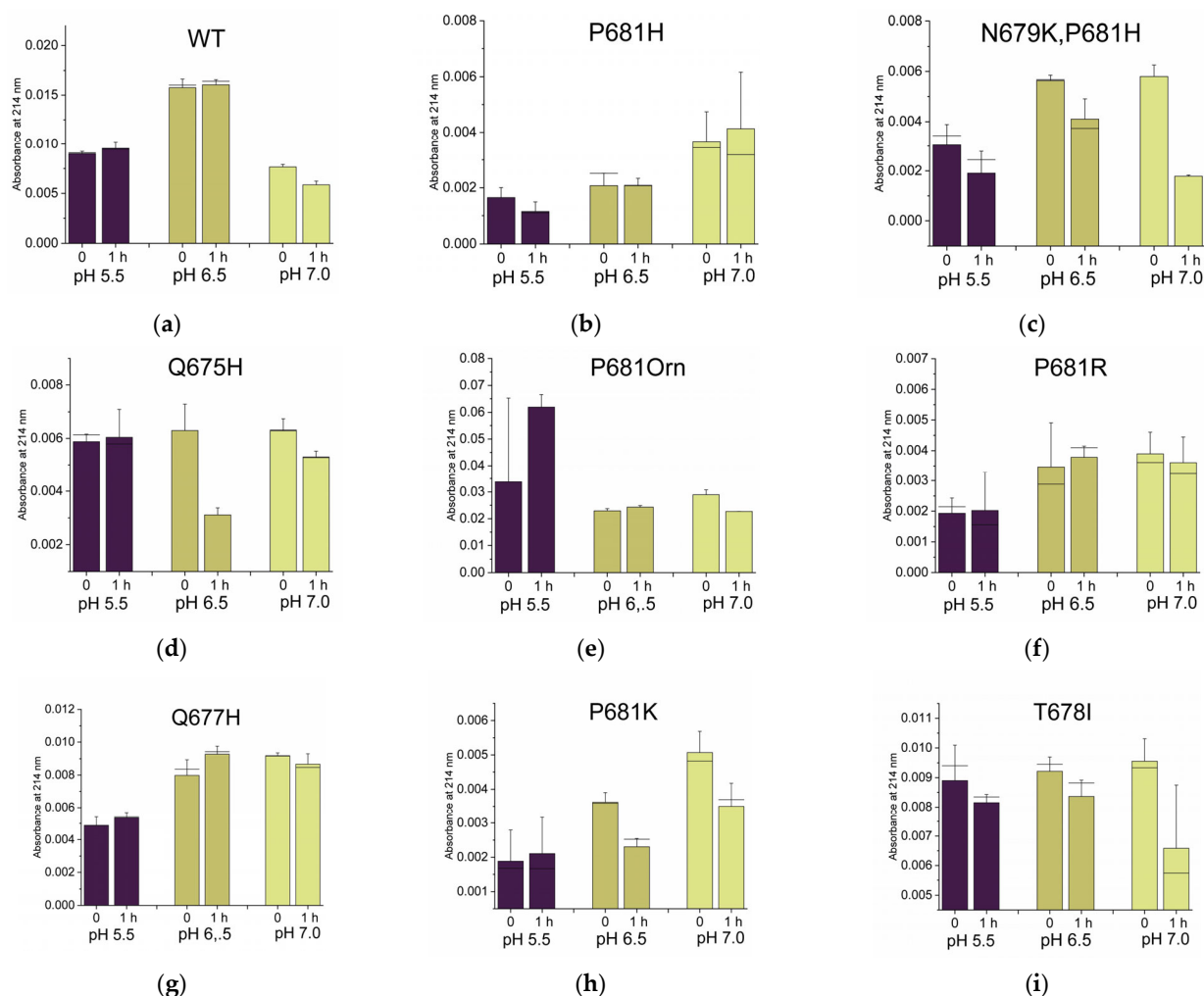


**Figure 7.** In vitro digestion of peptides mimicking the cleavage site (673–689) of SARS-CoV-2 S WT and mutants. Peptides were incubated with sFur as described in the Materials and Methods section. Areas relative to residual uncleaved peptide detectable by HPLC at 214 nm are reported. Experiments were performed as triplicates. Mean values and error bars are reported; (a) WT peptide; (b) P681H; (c) N679K/P681H; (d) Q675H; (e) P681Orn; (f) P681R; (g) Q677H; (h) P681K; (i) T678I mutant peptides.

### 2.2.3. Why Are There No P681K Variants of the SARS-CoV-2 Spike?

Position 681 of the envelope glycoprotein S of SARS-CoV-2 is being kept under monitoring since variants carrying mutations at this position have been linked to VOC forms of the virus. Originally, the envelope glycoprotein accommodated a proline residue at this position. Among Furin substrates, prolines are not very popular at the cleavage site because of their intrinsic rigid structure that confers restricted grades of freedom to the characteristic five-atom ring of proline. Accordingly, it is generally accepted that the substrates of Furin are characterized by a vast degree of flexibility, to allow optimal fitting into the catalytic site [74]. In this respect, it is not surprising that the proline at the 681 position is subject to replacements. Moreover, the mutations at this particular position further make the stretch more accessible since the close-by P681-dependent (O-)glycosylation, which may hamper the substrate–enzyme docking, is lost [53]. Overall, there is a clear pressure on the 681 position for the acquisition of a more suitable residue. P681R (Beta) and P681H (Delta/Omicron) are the most predominant over all possible amino acidic alternatives available (4407836 R; 6454096 H; 0 K; 2 D; 0 E; 8 Q; 36 N; 7 T; 129 S; 4 F; 826 Y; 0 W; 1685 L; 0 V; 0 I; 2 A; 28 C; 0 M; 10864663 TOT sequences deposited in GISAID database as of 30/08/2022). Intriguingly, no lysine has ever been reported to replace proline at 681, despite Arg, His and Lys sharing basic features. Indeed, the side chains of the three residues

are positively charged. We reasoned that Lys may not optimally fit the catalytic pocket of Furin due to its side chain, which may result in it being too long. To test this hypothesis, we synthesized two 17mer peptides encompassing the SARS-CoV-2 spike (P14-P4') region and bearing either the P681K or P681Orn mutation (Table 1). Ornithine is not an amino acid coded by DNA. Despite not being a building block of proteins, the residue is an important natural intermediate in metabolic processes of mammalian tissues. The ornithine side chain ( $-\text{[CH}_2\text{]}_3\text{-NH}_3^+$ ) closely resembles that of lysine ( $-\text{[CH}_2\text{]}_4\text{-NH}_3^+$ ), but it lacks a single  $-\text{CH}_2$  unit. That is, Orn is a “short version” of Lys. Peptides were digested and analyzed as reported above. We found that the P681Orn peptide behaved similarly to the WT at pH 7.0 and did not acquire cleavability in acidic conditions (Figure 7a vs. Figure 7e). On the other hand, P681K acquired cleavability at acidic pH values when compared to the WT (Figure 7a vs. Figure 7h). Overall, P681K performance was better than that of P681Orn and WT itself.

In conclusion, the presence of lysine instead of proline at position 681 may be beneficial in terms of peptide cleavability that becomes sensitive to mild acidic conditions. The length of the side chain of Lys may be crucial, given that the shorter ornithine analogue reverts the Lys phenotype. Overall, SARS-CoV-2 provides new insights on Furin specificity, also through the negative *in vivo* selection of specific mutations.

#### 2.2.4. Non-Conservative T678I Replacement Enhances Processing

The increase in basic residues around the scissile bond is compatible with the heavily positively charged surface of the catalytic pocket of Furin [75]. Within the SARS-CoV-2 spike, Arg/Lys/His replacements are preferentially found at odd positions and upstream of the main  $\text{RRAR}_{685}\downarrow$  motif. In contrast, hydrophobic residues are more representative for substitutions at the even positions (Figure 5). T678I replacement was detected early in 2020 [76] and it now represents one of the most frequent mutations after the Beta/Delta and Omicron variants (Figure S1). To our knowledge, no information is available regarding the impact of T678I on glycoprotein cleavage. To address this question, we synthesized the corresponding 17mer peptide (Table 1) that underwent digestion, as reported above. The substrate showed a two-fold cleavability increase with respect to the wild-type version at pH 7.0, and also some sensitivity to processing in acidic conditions (Figure 7a vs. Figure 7i).

Among all variants tested here, T678I stands as one of the best GOF mutants of the SARS-CoV-2 glycoprotein. Importantly, the data further suggest that combinations of specific amino acids can modulate the activity of Furin. More in detail, hydrophobicity—contrary to the expectations—can be a “plus” for substrate processing if strategically located upstream of the  $\text{RX}_n\text{R}\downarrow$  sequence.

#### 2.3. Conformational Investigations of the SARS-CoV-2 Wild-Type Cleavage Site and Its Mutants

Single mutations around the conserved  $\text{RRAR}\downarrow$  motif do greatly influence the processing event. In order to verify whether this phenomenon could be attributable to any conformational change, we performed Circular Dichroism (CD) and Attenuated Total Reflectance (ATR) Fourier transform–infrared spectroscopy (FT-IR) studies on the various peptides synthesized in our study (Figures 8 and 9). CD investigations in water suggest that the entire panel of sequences adopt no special conformation, demonstrating typical random CD profiles (Figure 8a). Accordingly, disordered proteins possess very low ellipticity above 210 nm and negative bands near 195 nm [77]. The flexibility of peptides is further evident when the latter are dissolved in trifluoroethanol (TFE), a solvent known to prompt helical structures. Here, we do observe the appearance of the characteristic  $\alpha$ -helix positive values below 200 nm and the negative peaks around 222 and 208 nm [78]. Peptides possessing mutations at 681 position are slightly red-shifted (Figure 8b).

CD analyses were complemented by ATR-FTIR investigations using lyophilized peptides. Spectra were collected in the  $400\text{--}4000\text{ cm}^{-1}$  range (Figure 9a). We focused our attention on amide I and II bands, which are the most characteristic absorptions in protein spectra (Figure 9b–g). Amide I is the result of the stretching vibrations of C=O and C-N

groups. Its frequency is found in the range between 1600 and 1700  $\text{cm}^{-1}$ . Amide II derives mainly from in-plane N-H bending and C-N/C-C stretching vibrations. It is found in the 1510 and 1580  $\text{cm}^{-1}$  regions. Overall, the exact band positions are due to the backbone conformation and the hydrogen bonding pattern (typically, 1623–1641  $\text{cm}^{-1}$   $\beta$ -sheet; 1642–1657  $\text{cm}^{-1}$  random coil; 1648–1657  $\text{cm}^{-1}$   $\alpha$ -helix; 1674–1695  $\text{cm}^{-1}$   $\beta$  sheet) [79]. We found that His containing peptides N677K/P681H, P681H and Q675H, but not Q677H, show an additional peak around 1618  $\text{cm}^{-1}$ . N677K/P681H and Q675H peptides are further characterized by an increased 1618/1650  $\text{cm}^{-1}$  ratio (Figure 9b). No clear shifts were detected in the 1480–1580  $\text{cm}^{-1}$  range (Figure 9c). When clustering the peptides according to mutation at position 681, we could observe that the replacement of WT proline with a basic residue (Lys, Arg, and Orn) did not grossly affect the ATR-FTIR profile in the 1580–1690  $\text{cm}^{-1}$  range (Figure 9d). However, the same mutations induced a variation within the 1480–1580  $\text{cm}^{-1}$  range, resulting in a major contribution of the band component, peaking at around 1537/40  $\text{cm}^{-1}$  (Figure 9e). No differences were evident in the case of the T678I peptide (Figure 9f,g).

Overall, the data at hand suggest that variants may acquire a certain degree of order when compared to the WT peptide sequence.

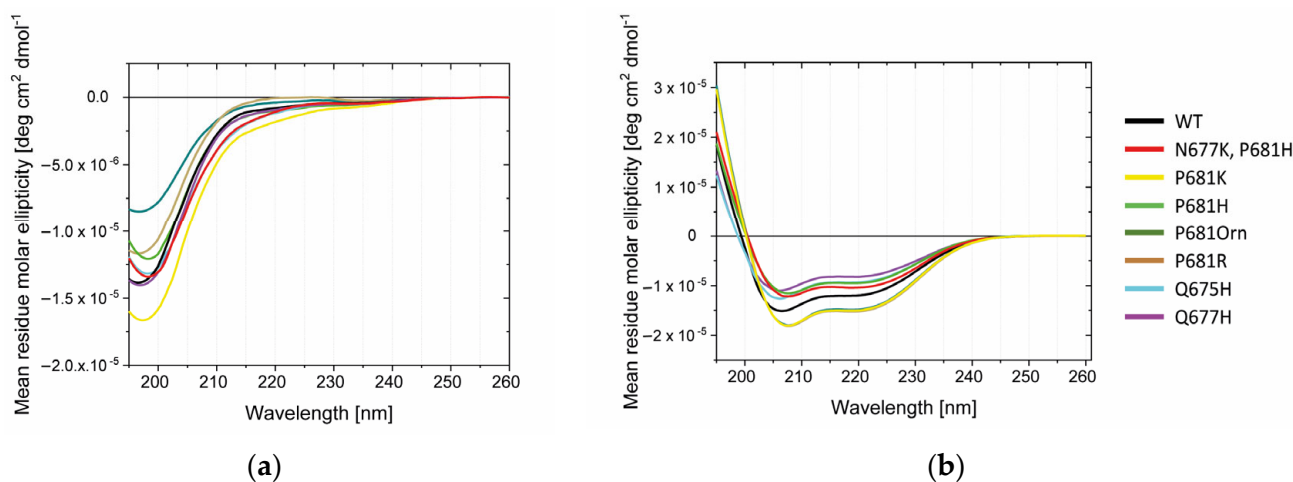
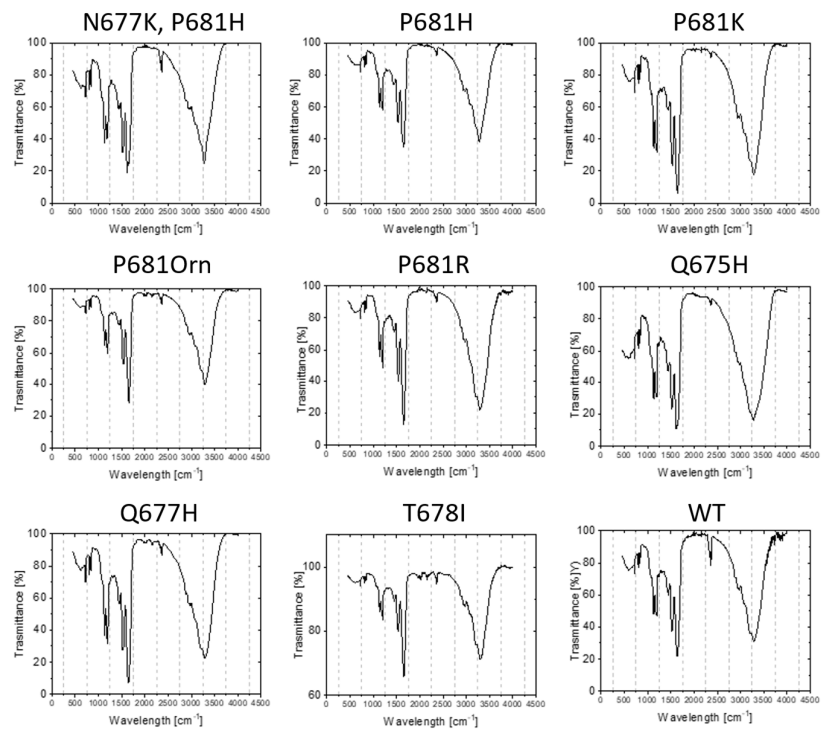
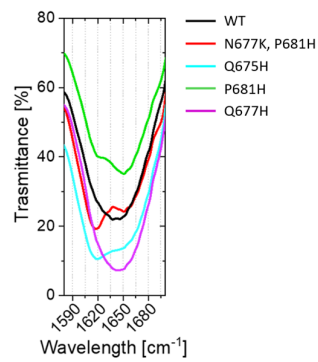


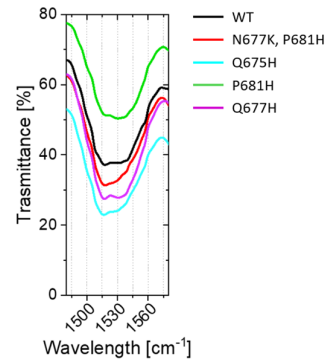
**Figure 8.** CD spectra of the SARS-CoV-2 S-derived peptides described in Table 1 in (a) water and (b) trifluoroethanol. Data are expressed as mean residue molar ellipticity (Raw data and calculations are reported in Supplementary Table S1).



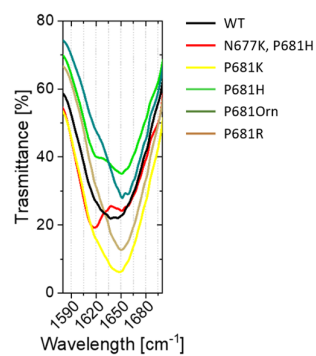
(a)



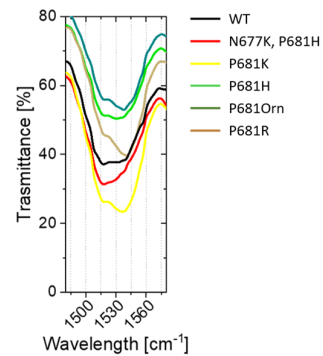
(b)



(c)



(d)



(e)

Figure 9. Cont.

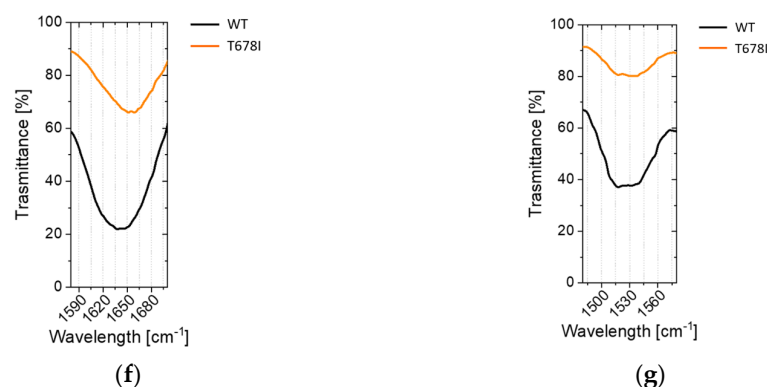


**Figure 9.** ATR-FTIR spectra of the SARS-CoV-2 S-derived peptides described in Table 1 (a) 400–4000  $\text{cm}^{-1}$ ; (b,d,f) 1580–1690  $\text{cm}^{-1}$ ; (c,e,g) 1480–1580  $\text{cm}^{-1}$ . (b,c) show His mutants vs. WT spectra; (d,e) show mutations at 681 vs. WT spectra; (f,g) show T678I vs. WT spectra.

#### 2.4. Sustainability

We are deeply engaged in sustainability. Being aware of the resources employed in our work is of great importance to better plan future experiments.

The entire project was monitored for the use of disposable plastics (Table 2). In parallel, ad hoc measures were adopted to minimize the impact of our work on the environment and non-renewable resources, whenever it was possible.

**Table 2.** Plastic items used in the current work and registered in our Green Book (GB).

Use	Object	Quantity	Unit Weight [g]	TOT Weight [g]
Peptide synthesis	PTFE filter 0.45 $\mu\text{m}$ (diameter 30 mm)	9	2.30	20.70
	PVDF filter 0.45 $\mu\text{m}$ (diameter 13 mm)	9	12.00	108.00
	Reactor	9	4.00	36.00
	Syringe (1 mL)	9	2.20	19.80
	Syringe (20 mL)	12	10.00	120.00
	Tips (200 $\mu\text{L}$ )	100	0.27	27.00
	Tips (20 $\mu\text{L}$ )	100	0.12	12.00
	Tube (1.5 mL)	40	1.00	40.00
	Tube (2 mL)	10	1.15	11.50
	Tube (50 mL)	40	12.70	508.00
	Tube (6 mL)	30	3.50	105.00
	Glove pairs	9	2.30	20.70
	Flask (125 $\text{cm}^2$ )	1	100.00	100.00
Flask (250 $\text{cm}^2$ )	1	200.00	200.00	
Flask (75 $\text{cm}^2$ )	6	60.00	360.00	
In vitro—conformation studies	Plate (24 well)	16	65.40	1046.40
	Plate (48 well)	3	56.00	168.00
	Plate (96 well)	3	64.60	193.80
	Sterile pipette (10 mL)	80	14.00	1120.00
	Sterile pipette (25 mL)	15	15.60	234.00
	Sterile pipette (2 mL)	2	4.40	8.80
	Sterile pipette (5 mL)	60	7.90	474.00
	Tips (10 $\mu\text{L}$ )	100	0.12	12.00
	Tips (1000 $\mu\text{L}$ )	200	0.76	152.00
	Tips (200 $\mu\text{L}$ )	1500	0.27	405.00
	Tube (1.5 mL)	1000	1.00	1000.00
	Tube (15 mL)	15	6.40	96.00
	Tube (50 mL)	30	12.70	381.00
	Glove pairs	200	6.20	1240.00
	Other			
			<b>TOT</b>	<b>9819.00</b>

According to our “Green Book” (GB) summary, we required approximately 10 kg of plastics that were disposed as recyclable resources only in part (10%). The rest was stocked as hazardous materials for the following treatment, as stated by Italian laws. During the realization of this study, we replaced some plastics with equivalent glass items, focusing on those steps where it was more necessary. For example, we opted for re-usable glass vials to collect purified peptides and monitor digestions by HPLC. Despite one single HPLC vial weighing only 0.1 g and one single collecting tube weighing only a few grams, since we ran hundreds of independent analyses, it is clear that we saved considerable plastic waste.

We believe that researchers must become more aware of the disposable items that are used in their laboratory on a routine basis. A simple diary (e.g., GB) reporting a rough estimation of plastics use may be useful for visualizing possible weaknesses, allowing researchers to intervene with greener alternatives.

### 3. Discussion

SARS-CoV-2 is the etiological agent of COVID-19, the current pandemic claiming millions of lives. Due to the SARS-CoV-2 spread worldwide and its massive propagation, the pathogen has the chance to grossly mutate and eventually adapt to the human host. Following the initial waves of infection, the pathogen has shifted towards variants with adaptive advantage over previous strains [8–10,80]. In this work, we have focused our attention on specific mutations located at the S1–S2 boundary of the envelope glycoprotein S.

To be functional, the virus requires the maturation of the glycoprotein S by cleavage at the  ${}_{682}\text{RRAR}\downarrow\text{S}_{686}$  motif by Furin. The presence of a multi-basic site distinguishes SARS-CoV-2 from SARS-CoV and all other known sarbecoviruses whose S protein is not cleaved by Furin-like proteases [80,81]. The processing was shown to decrease the overall stability of the SARS-CoV-2 glycoprotein when compared to the S protein of a closely related bat virus (RaTG13) lacking the Furin cleavage site (CS). In turn, this implied the easier adoption of the open conformation required for SARS-CoV-2 S to bind to the human ACE2 receptor. Indeed, RaTG13 virus would not be able to interact with the human receptor efficiently and would thus be unlikely to infect humans directly [4]. Another important aspect of the CS is its dependence on Furin—a ubiquitous protease—which enables SARS-CoV-2 to replicate in virtually any organ, allowing massive human body infection. Importantly, the virus has not been reported to escape from Furin in vivo, despite this being shown to be readily feasible in vitro [40].

Based on these premises, the appearance of the Furin cleavage site within the SARS-CoV-2 glycoprotein has been a key event that has drastically shaped its properties. Of course, strictly monitoring likely modifications around the cleavage site is of great importance because any variation may have a significant impact on virus infectivity and tropism. As for other viral sequences, the region around the processing site has evolved and acquired multiple mutations over time. By analyzing the GISAID sequence database, we could observe that the polybasic cluster is rather conserved. Our report is perfectly in line with the evidence that SARS-CoV-2 continues to prefer Furin, a protease that cleaves substrates after  $\text{BX}_n\text{B}\downarrow$  (B, basic residue; X, any residue but Cys). Despite the phenomenon having no clear explanation, it somehow resembles the case of the Ebola virus (EBOV) glycoprotein, which is cleaved by Furin as well. Ebola virus glycoprotein cleavage by Furin is not critical for virus replication in vitro and infectivity and virulence in non-human primates [82], and the polybasic motif is highly conserved among different strains and isolates. In contrast to the conservation of the motif  ${}_{682}\text{RRAR}\downarrow\text{S}_{686}$ , surrounding residues are much more likely to vary. In particular, replacements with hydrophilic amino acids are preferred at P positions and hydrophobic amino acids are preferred at P' positions. The exact pattern of mutations, as well as the identity of the residues, seems to be everything but random, e.g., position 681 accommodates His or Arg but never Lys, despite the latter sharing similar basic features when compared to the first two. In line with the evidence reported by other groups, we found that many peptides mimicking the processing site of variants possess a gain-of-function phenotype in terms of cleavability. Likely, the mutants

do better match their partner, that is, the Furin enzyme. Of note, the Omicron N679K, P681H peptide was shown to be the most cleavable substrate among those tested here. Interestingly, position 681 of the S glycoprotein is five residues far from the scissile bond (P5 position). Accordingly, substrates carrying basic amino acids at the P5 position were recently shown to outperform any other alternative when interacting with the Furin catalytic pocket [83]. The contribution of K679 cannot be underestimated, either. On the other hand, we showed that the P681K peptide possesses a gain-of-function phenotype, although this mutation has never been reported in the GISAID database. The reason why certain amino acids—e.g., the *in vitro* gain-of-function K681—are not viable among the circulating SARS-CoV-2 variants remains elusive. This suggests that the amino acid at this peculiar position may be involved in functions other than modulating the propensity to cleavage by Furin. Accordingly, the cleavage site functions as a binding motif to alternative receptors [80]. In addition, we cannot exclude that the presence of Lys at position 681 may be detrimental for the overall glycoprotein arrangement, which would lose the optimal affinity for the major receptor: the ACE2 protein [4,80,84]. Finally, there is a mutation—T678I—placed very far away from the actual processing site (R<sub>685</sub>↓) that is able to greatly affect cleavability. It is noteworthy to highlight the hydrophobic nature of this replacement.

The peculiar position and nature of T678I suggest that the Furin consensus sequence BX<sub>n</sub>B↓ represents a minimal recognition motif where all surrounding regions are able to modulate the extent of processing. This is further supported by the distant Q677H and Q675H mutations that provide key information regarding the way Furin works. Interestingly, Q675H increases the substrate cleavability at acidic conditions, whereas the nearby Q677H does not. Of note, we observed minimal changes on the residues after the cleavage site. We may conclude that P' positions are not as important as P positions since they did not require any gross refinement, that is, the introduction of amino acids different from those found in the wild-type sequence. From a different point of view, the actual residues may be the best Furin option and any replacement may result in a loss-of-function variant. Along these lines, known Furin substrates privilege hydrophobic amino acids at P1' and P2' positions, as is the case of the SARS-CoV-2 spike cleavage site.

The question of whether mutations also impact CS conformation still remains open. We found that stretch 673–689 of the glycoprotein S adopts no specific structure in aqueous environments, both in the case of WT and variant peptides. This is in line with the evidence that this region is not visible in the resolved crystal structure [4], further suggesting a high degree of backbone flexibility. The finding is not surprising since the region around the scissile bond is normally thought to be able to match the enzyme by adapting to the rigid structure of the catalytic pocket. However, we observed that some mutations—in particular those introducing a histidine residue—induce a shift in the recorded ATR-FTIR and CD spectra. Despite the variation not speaking for a clear-cut conformational change, the data at hand suggest that the population of conformers may be different in the case of the mutations, and in turn this could impact catalytic pocket/interaction. Interestingly, recent studies on Furin revealed that the enzyme can shape multiple conformations. Each single state does not exist *per se*, but it is generated by the interactions with specific substrates/inhibitors [66]. Thus, the way each peptide is recognized by the enzyme may be different, and the ultimate structure of the peptide bound to Furin CS may be unique and not predictable by simple modelling. However, the picture is much more complex, and the data collected here are insufficient to fully explain the increase in specific combinations of amino acids but not others. In fact, we need to keep in mind that the glycoprotein S has multiple functions and the stretch encompassing the cleavage site may be involved in activities unrelated to spike maturation. Finally, we cannot exclude that the introduction of amino acids—other than those actually found—at the cleavage site may be well tolerated in terms of Furin cleavability but may likewise create new unwanted functions that are detrimental for virus propagation.

## 4. Materials and Methods

### 4.1. sFurin and SARS-CoV-2 S Production

sFurin consists of a soluble form of hFurin truncated before the transmembrane domain [85], whereas the SARS-CoV-2 S protein lacks the transmembrane region [4]. sFurin and SARS-CoV-2 S proteins were produced in HEK293 F cells (Human Embryonic Kidney cells) and grown in suspension in FreeStyle™ 293 Expression Medium (Gibco, ThermoFisher) in shaking (130 rpm) flasks, without antibiotics, at 37 °C and 8% CO<sub>2</sub>. In detail, cells were sub-cultured every four days to  $0.3 \times 10^6$  cells/mL density and brought to final 1 L at  $1 \times 10^6$  cells/mL for transfection by polyethylenimine (PEI). Briefly, for 1 mL of culture, 3 µg of PEI and 1 µg of DNA were resuspended in 20 mL of Opti-MEM (Gibco, ThermoFisher) each, separately. The two solutions were incubated for 15 min at room temperature (RT) prior to mixing together. Following a further 15 min, the final solution was added drop-wise to the cell culture under stirring. Cells were incubated at 37 °C, 8% CO<sub>2</sub> for four days prior to media collection. Cells were removed by centrifugation ( $6000 \times g$  for 20 min at 4 °C (Backman Coulter® Avanti® 25, rotor JLA 9.1000). Supernatants were aliquoted and stored at −80 °C (sFur) or further treated for purification (SARS-CoV-2 spike). SARS-CoV-2 S protein supernatant was filtered (0.45 µm) prior to injection into a Ni Excell column (CV = 3mL) pre-equilibrated in buffer A (25 mM Tris pH 8, 150 mM NaCl, 10 mM Imidazole). Protein elution was achieved by treating with 4mL of 60% buffer B (25 mM Tris pH 8, 150 mM NaCl, 500 mM Imidazole). The purity grade of SARS-CoV-2 S protein was assessed by SDS-PAGE gel and Coomassie stain.

### 4.2. In Vitro SARS-CoV-2 S Digestion

Protein concentration was assessed by nanodrop. Buffers: 20 mM CaCl<sub>2</sub>, 250 mM Sodium acetate, pH 5.5; 20 mM CaCl<sub>2</sub>, 250 mM HEPES (4-(2-hydroxyethyl)-1-piperazineethanesulfonic acid), pH 7.0; and 20 mM CaCl<sub>2</sub>, 250 mM Tris-HCl, pH 8. A supernatant of cells overexpressing sFur was used as the source of enzymes. Then, 1.5 µg of SARS-CoV-2 S glycoprotein was diluted in suitable buffer to a final 150 µL in the presence of 20 µL of sFur and 20 µL of buffers. For each time point, 36 µL of digestion solution was collected, mixed with 4 µL of ethylenediaminetetraacetic acid/ethylene glycol-bis(β-aminoethyl ether)-N,N,N',N'-tetraacetic acid (EDTA/EGTA) 500 mM, and heated at 95 °C for 5 min. All samples were frozen at −80 °C prior to a final Western blotting analysis.

### 4.3. Western Blot

Protein samples were treated with Laemmli buffer and incubated for 5 min at 95 °C prior to loading to gels. Protein weights were determined using a Prestained Protein MW Marker (Thermo Scientific, Waltham, MA, USA). Electrophoresis was performed in SurePAGE™ Bis-Tris (4–20%) precast gels (GenScript Biotech, Rijswijk, Netherlands) and Tris-MOPS buffer (pH 7.5). Transfer was carried out in a semi-dry condition from SDS-PAGE to a nitrocellulose membrane, using a Bio-Rad Trans-Blot Turbo Transfer System (90 V for 90 min). Transferred proteins were detected with an anti-His HRP conjugation (Abcam, Cambridge, UK 1:4000). Images were processed with Fiji (ImageJ, <https://imagej.net/>).

### 4.4. Peptide Synthesis

All peptides were synthesized by solid-phase peptide synthesis (SPPS) techniques (Syro I, Multisynthec, Witten, Germany) using Fmoc-chemistry. Amino acid side-chain protections were: t-Butyl—(tBu)- for Ser, Thr, and Tyr; trityl (Trt)- for Asn and Gln; 2,2,4,6,7-pentamethylidihydrobenzofuran-5-sulfonyl group (Pbf) for Arg. As solid support, the rink amide resin (0.52 mmol/g; scale 0.1 mmol) was used. The cleavage of the newly synthesized peptides from the resin and the side-chain global deprotection was achieved by treatment with 5 mL of 2.5% H<sub>2</sub>O MilliQ, 2.5% Triethylsilane (TES), and 95% Trifluoroacetic acid (TFA) for 90 min. Crude peptides were filtered out from concentrated TFA solution and precipitated with cold ethyl ether. Approximately 30 mg of each crude peptide was purified by semi-preparative HPLC in the following conditions: column Zorbax 300SB-C18

(5  $\mu\text{m}$ , 300  $\text{\AA}$ , 9.4  $\times$  250 mm, Agilent, Santa Clara, CA, USA); eluent A, 0.05% TFA in MilliQ water; eluent B, 0.05% TFA in  $\text{CH}_3\text{CN}$ ; gradient, 0% to 40%B in 40 min; flow rate, 4 mL/min; and detection UV absorption at 214nm. Peptide purity grade was assessed by analytical HPLC to be  $\geq 97\%$  (Vydac 218TP C18 (5  $\mu\text{m}$ , 300  $\text{\AA}$ , 4.6  $\times$  250 mm, Grace, Columbia, SC, USA); injection volume, 20  $\mu\text{L}$  of 1mg/mL peptide; eluent A, 0.05%TFA in  $\text{H}_2\text{O}$  milliQ; eluent B, 0.05% TFA in  $\text{CH}_3\text{CN}$ ; gradient, 0–20% B in 40 min; and UV detection at 214 nm). The identity of the peptides was assessed by MALDI mass spectrometry (Table 1).

#### 4.5. Peptide In Vitro Digestions

Aqueous peptide stocks were prepared at 5 mM. Buffers and sFur, as described in paragraph 4.2., 2  $\mu\text{L}$  of peptide stock solutions, 20  $\mu\text{L}$  of sFur, and 20  $\mu\text{L}$  of suitable buffer were mixed in  $\text{H}_2\text{O}$  MilliQ up to a 150  $\mu\text{L}$  final volume. Then, 20  $\mu\text{L}$  of samples was collected at the indicated time points and treated as described in paragraph 4.2. All samples were analyzed by HPLC—Vydac Column 218TP C18 (5  $\mu\text{m}$ , 300 $\text{\AA}$ , 4.6  $\times$  250 mm, Grace, Columbia, SC, USA); injection volume, 20  $\mu\text{L}$  reaction mix; eluent A, 0.05%TFA in  $\text{H}_2\text{O}$  milliQ; eluent B, 0.05% TFA in  $\text{CH}_3\text{CN}$ ; gradient, 0–20% B in 40 min; and UV detection at 214 nm.

#### 4.6. Circular Dichroism (CD) Analyses

CD measurements were realized with a spectropolarimeter Jasco J-810 at 25  $^\circ\text{C}$ . The CD signal was monitored at 0.2 nm intervals from 260 nm to 195 nm with a scan speed of 100 nm/min in a 0.1 mm quartz path cuvette, registering ten scans. Peptides were dissolved in acidic buffer (25 mM Sodium Acetate pH 5.5, 2 mM  $\text{CaCl}_2$ ) and 100% Trifluoroethanol (TFE), at a concentration of 50  $\mu\text{M}$ . The data reported are the average of ten scans, subtracting the background obtained by a blank of either buffer only or 100%.

#### 4.7. Attenuated Total Reflectance Fourier-Transform Infrared Spectroscopy Investigation

Lyophilized peptides were analyzed with a Jasco FT/IR -4700 instrument equipped with an ATR-PRO ONE diamond accessory. The system resolution was 0.8  $\text{cm}^{-1}$ . Samples were placed on the cell measurer and scanned from 4000 to 400  $\text{cm}^{-1}$ . For each sample, 40 scans were run at room temperature.

## 5. Conclusions

In summary, we investigated the cleavage site of the SARS-CoV-2 glycoprotein and found that circulating strains evolved specific mutations over others. In general, hydrophilic replacements are more common among the positions before the scissile bond, whereas hydrophobic amino acids are more representative of the positions after the cleavage site. In order to understand the impact of specific amino acid replacements on cleavage efficiency, peptides encompassing the spike scissile stretch and carrying the most representative variants were synthesized and digested with Furin in vitro. Mutations generally make the peptide easier to cut. The Omicron-derived N679K, P681H double mutant was found to be a superior substrate for Furin, thus supporting the large spread of this variant among the worldwide population. In addition, we provide the first evidence suggesting that the increase in specific mutations but not others is not only due to the selection of better cleavable Furin substrates. Indeed, despite being cleaved in vitro, the P681K variant has never been reported, supporting a more complex role of the cleavage site during infection. Moreover, for the first time, we provide some information on the structure of this specific region, which seems to be random in aqueous solutions. Despite no peculiar structural motifs being present, replacements of the WT residues with other amino acids induce a likely change in the conformer population.

From the point of view of the Furin enzyme, the emergence of variants carrying specific amino acid replacements at the cleavage site provides important information on protease substrate specificity. Indeed, despite the minimal Furin consensus sequence  $\text{BX}_n\text{B}_d$  being well accepted, little is known about the surrounding amino acids that may influence

Furin's ability to cleave its substrates. During the pandemic, the SARS-CoV-2 virus has generated a tremendous number of variants, virtually scanning any possible combination of residues at the cleavage site. Those that provided a gain-of-function phenotype—that is, a better cleavability—have been selected. However, as discussed above, we need to keep in mind that some mutations may have never seen the light of the day because of reasons unrelated to Furin processing.

Further investigations are required to understand the importance of these findings in the context of the full-length SARS-CoV-2 glycoprotein. The entire spike often carries multiple mutations that are not limited to the cleavage site. These additional mutations may be critical for understanding the overall impact of the amino acid replacement studied here.

**Supplementary Materials:** The following supporting information can be downloaded at: <https://www.mdpi.com/article/10.3390/ijms24054791/s1>.

**Author Contributions:** Conceptualization, A.P. (Antonella Pasquato), M.D. and L.C. (Laura Cendron); methodology, A.P. (Antonella Pasquato), M.D., L.C. (Laura Cendron), S.R. and A.P. (Angela Pavan); validation, L.C. (Leonardo Cassari), A.P. (Angela Pavan), M.C., E.Z. and A.P. (Antonella Pasquato); formal analysis, A.P. (Angela Pavan), L.C. (Leonardo Cassari), A.P. (Antonella Pasquato) and M.C.; investigation, A.P. (Angela Pavan), L.C. (Leonardo Cassari), G.Z., M.C., E.Z., A.G. and A.P. (Antonella Pasquato); resources, A.P. (Antonella Pasquato); data curation, A.P. (Antonella Pasquato), L.C. (Leonardo Cassari) and A.P. (Angela Pavan); writing—original draft preparation, A.P. (Antonella Pasquato); writing—review and editing, A.P. (Antonella Pasquato), M.D., L.C. (Laura Cendron), L.C. (Leonardo Cassari), G.Z., A.P. (Angela Pavan), E.Z., M.C., A.G. and S.R.; supervision, A.P. (Antonella Pasquato), M.D. and L.C. (Laura Cendron); project administration, A.P. (Antonella Pasquato); funding acquisition, A.P. (Antonella Pasquato), M.D. and L.C. (Laura Cendron). All authors have read and agreed to the published version of the manuscript.

**Funding:** This research was funded by the EU Research Framework Programme H2020/Marie Skłodowska-Curie Actions, grant number 101024974.

**Institutional Review Board Statement:** Not applicable.

**Informed Consent Statement:** Not applicable.

**Data Availability Statement:** Not applicable.

**Acknowledgments:** We acknowledge Nabil G. Seidah for kindly providing the plasmid encoding for a soluble form of hFurin truncated before the transmembrane domain and Anthony Wrobe for shearing the plasmid encoding for the SARS-CoV-2 S protein ectodomain.

**Conflicts of Interest:** The authors declare no conflict of interest.

## References

1. Coronaviridae Study Group of the International Committee on Taxonomy of Viruses. The Species Severe Acute Respiratory Syndrome-Related Coronavirus: Classifying 2019-NCoV and Naming It SARS-CoV-2. *Nat. Microbiol.* **2020**, *5*, 536. [[CrossRef](#)]
2. Boni, M.F.; Lemey, P.; Jiang, X.; Lam, T.T.-Y.; Perry, B.W.; Castoe, T.A.; Rambaut, A.; Robertson, D.L. Evolutionary Origins of the SARS-CoV-2 Sarbecovirus Lineage Responsible for the COVID-19 Pandemic. *Nat. Microbiol.* **2020**, *5*, 1408–1417. [[CrossRef](#)] [[PubMed](#)]
3. Wan, Y.; Shang, J.; Graham, R.; Baric, R.S.; Li, F. Receptor Recognition by the Novel Coronavirus from Wuhan: An Analysis Based on Decade-Long Structural Studies of SARS Coronavirus. *J. Virol.* **2020**, *94*, e00127–e20. [[CrossRef](#)] [[PubMed](#)]
4. Wrobel, A.G.; Benton, D.J.; Xu, P.; Roustan, C.; Martin, S.R.; Rosenthal, P.B.; Skehel, J.J.; Gamblin, S.J. SARS-CoV-2 and Bat RaTG13 Spike Glycoprotein Structures Inform on Virus Evolution and Furin-Cleavage Effects. *Nat. Struct. Mol. Biol.* **2020**, *27*, 763–767. [[CrossRef](#)]
5. Herrera-Esposito, D.; de los Campos, G. Age-Specific Rate of Severe and Critical SARS-CoV-2 Infections Estimated with Multi-Country Seroprevalence Studies. *BMC Infect. Dis.* **2022**, *22*, 311. [[CrossRef](#)] [[PubMed](#)]
6. Dhar, D.; Mohanty, A. Gut Microbiota and Covid-19- Possible Link and Implications. *Virus Res.* **2020**, *285*, 198018. [[CrossRef](#)]
7. Rishi, P.; Thakur, K.; Vij, S.; Rishi, L.; Singh, A.; Kaur, I.P.; Patel, S.K.S.; Lee, J.-K.; Kalia, V.C. Diet, Gut Microbiota and COVID-19. *Indian J. Microbiol.* **2020**, *60*, 420–429. [[CrossRef](#)]
8. Zahradník, J.; Nunvar, J.; Schreiber, G. Perspectives: SARS-CoV-2 Spike Convergent Evolution as a Guide to Explore Adaptive Advantage. *Front. Cell. Infect. Microbiol.* **2022**, *12*, 748948. [[CrossRef](#)]

9. Thakur, V.; Bhola, S.; Thakur, P.; Patel, S.K.S.; Kulshrestha, S.; Ratho, R.K.; Kumar, P. Waves and Variants of SARS-CoV-2: Understanding the Causes and Effect of the COVID-19 Catastrophe. *Infection* **2022**, *50*, 309–325. [[CrossRef](#)]
10. Zhou, W.; Wang, W. Fast-Spreading SARS-CoV-2 Variants: Challenges to and New Design Strategies of COVID-19 Vaccines. *Signal Transduct. Target. Ther.* **2021**, *6*, 226. [[CrossRef](#)]
11. Luo, W.-R.; Wu, X.-M.; Wang, W.; Yu, J.-L.; Chen, Q.-Q.; Zhou, X.; Huang, X.; Pan, H.-F.; Liu, Z.-R.; Gao, Y.; et al. Novel Coronavirus Mutations: Vaccine Development and Challenges. *Microb. Pathog.* **2022**, *173*, 105828. [[CrossRef](#)]
12. Wang, R.; Simoneau, C.R.; Kulsuptrakul, J.; Bouhaddou, M.; Travisano, K.A.; Hayashi, J.M.; Carlson-Stevermer, J.; Zengel, J.R.; Richards, C.M.; Fozouni, P.; et al. Genetic Screens Identify Host Factors for SARS-CoV-2 and Common Cold Coronaviruses. *Cell* **2021**, *184*, 106–119.e14. [[CrossRef](#)] [[PubMed](#)]
13. Santopolo, S.; Riccio, A.; Santoro, M.G. The Biogenesis of SARS-CoV-2 Spike Glycoprotein: Multiple Targets for Host-Directed Antiviral Therapy. *Biochem. Biophys. Res. Commun.* **2021**, *538*, 80–87. [[CrossRef](#)] [[PubMed](#)]
14. Shang, J.; Wan, Y.; Luo, C.; Ye, G.; Geng, Q.; Auerbach, A.; Li, F. Cell Entry Mechanisms of SARS-CoV-2. *Proc. Natl. Acad. Sci. USA* **2020**, *117*, 11727. [[CrossRef](#)]
15. Peacock, T.P.; Goldhill, D.H.; Zhou, J.; Baillon, L.; Frise, R.; Swann, O.C.; Kugathasan, R.; Penn, R.; Brown, J.C.; Sanchez-David, R.Y.; et al. The Furin Cleavage Site in the SARS-CoV-2 Spike Protein Is Required for Transmission in Ferrets. *Nat. Microbiol.* **2021**, *6*, 899–909. [[CrossRef](#)] [[PubMed](#)]
16. Bestle, D.; Heindl, M.R.; Limburg, H.; Van Lam van, T.; Pilgram, O.; Moulton, H.; Stein, D.A.; Hards, K.; Eickmann, M.; Dolnik, O.; et al. TMPRSS2 and Furin Are Both Essential for Proteolytic Activation of SARS-CoV-2 in Human Airway Cells. *Life Sci. Alliance* **2020**, *3*, e202000786. [[CrossRef](#)] [[PubMed](#)]
17. Essalmani, R.; Jain, J.; Susan-Resiga, D.; Andréo, U.; Evagelidis, A.; Derbali, R.M.; Huynh, D.N.; Dallaire, F.; Laporte, M.; Delpal, A.; et al. Distinctive Roles of Furin and TMPRSS2 in SARS-CoV-2 Infectivity. *J. Virol.* **2022**, *96*, e0012822. [[CrossRef](#)] [[PubMed](#)]
18. Cheng, Y.-W.; Chao, T.-L.; Li, C.-L.; Chiu, M.-F.; Kao, H.-C.; Wang, S.-H.; Pang, Y.-H.; Lin, C.-H.; Tsai, Y.-M.; Lee, W.-H.; et al. Furin Inhibitors Block SARS-CoV-2 Spike Protein Cleavage to Suppress Virus Production and Cytopathic Effects. *Cell Rep.* **2020**, *33*, 108254. [[CrossRef](#)] [[PubMed](#)]
19. Seidah, N.G.; Prat, A. The Biology and Therapeutic Targeting of the Proprotein Convertases. *Nat. Rev. Drug Discov.* **2012**, *11*, 367–383. [[CrossRef](#)]
20. Stout, A.E.; Guo, Q.; Millet, J.K.; Whittaker, G.R. Viral and Host Attributes Underlying the Origins of Zoonotic Coronaviruses in Bats. *Comp. Med.* **2021**, *71*, 442–450. [[CrossRef](#)]
21. Johnson, B.A.; Xie, X.; Kalveram, B.; Lokugamage, K.G.; Muruato, A.; Zou, J.; Zhang, X.; Juelich, T.; Smith, J.K.; Zhang, L.; et al. Furin Cleavage Site Is Key to SARS-CoV-2 Pathogenesis. *bioRxiv* **2020**. [[CrossRef](#)]
22. Böttcher-Friebertshäuser, E.; Klenk, H.-D.; Garten, W. Activation of Influenza Viruses by Proteases from Host Cells and Bacteria in the Human Airway Epithelium. *Pathog. Dis.* **2013**, *69*, 87–100. [[CrossRef](#)]
23. Kido, H. Influenza Virus Pathogenicity Regulated by Host Cellular Proteases, Cytokines and Metabolites, and Its Therapeutic Options. *Proc. Jpn. Acad. Ser. B Phys. Biol. Sci.* **2015**, *91*, 351–368. [[CrossRef](#)] [[PubMed](#)]
24. Coutard, B.; Valle, C.; de Lamballerie, X.; Canard, B.; Seidah, N.G.; Decroly, E. The Spike Glycoprotein of the New Coronavirus 2019-nCoV Contains a Furin-like Cleavage Site Absent in CoV of the Same Clade. *Antivir. Res.* **2020**, *176*, 104742. [[CrossRef](#)] [[PubMed](#)]
25. Zhang, T.; Wu, Q.; Zhang, Z. Probable Pangolin Origin of SARS-CoV-2 Associated with the COVID-19 Outbreak. *Curr. Biol.* **2020**, *30*, 1346–1351.e2. [[CrossRef](#)] [[PubMed](#)]
26. Wu, Y.; Zhao, S. Furin Cleavage Sites Naturally Occur in Coronaviruses. *Stem Cell Res.* **2021**, *50*, 102115. [[CrossRef](#)]
27. Chan, Y.A.; Zhan, S.H. The Emergence of the Spike Furin Cleavage Site in SARS-CoV-2. *Mol. Biol. Evol.* **2022**, *39*, msab327. [[CrossRef](#)]
28. Jaimes, J.A.; Millet, J.K.; Whittaker, G.R. Proteolytic Cleavage of the SARS-CoV-2 Spike Protein and the Role of the Novel S1/S2 Site. *iScience* **2020**, *23*, 101212. [[CrossRef](#)]
29. Mishra, S.; Mindermann, S.; Sharma, M.; Whittaker, C.; Mellan, T.A.; Wilton, T.; Klapsa, D.; Mate, R.; Fritzsche, M.; Zambon, M.; et al. Changing Composition of SARS-CoV-2 Lineages and Rise of Delta Variant in England. *eClinicalMedicine* **2021**, *39*, 101064. [[CrossRef](#)]
30. Zhao, L.P.; Lybrand, T.; Gilbert, P.; Payne, T.H.; Pyo, C.-W.; Geraghty, D.; Jerome, K. Rapidly Identifying New Coronavirus Mutations of Potential Concern in the Omicron Variant Using an Unsupervised Learning Strategy. *Res. Sq.* **2022**, *12*, 1–16. [[CrossRef](#)]
31. Winstone, H.; Lista, M.J.; Reid, A.C.; Bouton, C.; Pickering, S.; Galao, R.P.; Kerridge, C.; Doores, K.J.; Swanson, C.M.; Neil, S.J.D. The Polybasic Cleavage Site in SARS-CoV-2 Spike Modulates Viral Sensitivity to Type I Interferon and IFITM2. *J. Virol.* **2021**, *95*, e02422-20. [[CrossRef](#)] [[PubMed](#)]
32. Michihito, S.; Shinsuke, T.; Yukari, I.; Herman, M.C.; Mai, K.; Koshiro, T.; Kittiya, I.; Kentaro, U.; Takao, S.; Akihiko, S.; et al. SARS-CoV-2 Bearing a Mutation at the S1/S2 Cleavage Site Exhibits Attenuated Virulence and Confers Protective Immunity. *mBio* **2021**, *12*, e0141521. [[CrossRef](#)]
33. Johnson, B.A.; Xie, X.; Bailey, A.L.; Kalveram, B.; Lokugamage, K.G.; Muruato, A.; Zou, J.; Zhang, X.; Juelich, T.; Smith, J.K.; et al. Loss of Furin Cleavage Site Attenuates SARS-CoV-2 Pathogenesis. *Nature* **2021**, *591*, 293–299. [[CrossRef](#)] [[PubMed](#)]

34. Qiao, B.; de la Cruz, M.O. Enhanced Binding of SARS-CoV-2 Spike Protein to Receptor by Distal Polybasic Cleavage Sites. *ACS Nano* **2020**, *14*, 10616–10623. [[CrossRef](#)]
35. Ludovico, C.-C.; Ravi, O.; Liliana, P.; Minou, D.; Jonas, F.; Suvi, K.; van der Meer, F.; Katri, K.; Tuğberk, K.; Maria, A.; et al. Neuropilin-1 Facilitates SARS-CoV-2 Cell Entry and Infectivity. *Science* **2020**, *370*, 856–860. [[CrossRef](#)]
36. Cagno, V.; Tseligka, E.D.; Jones, S.T.; Tapparel, C. Heparan Sulfate Proteoglycans and Viral Attachment: True Receptors or Adaptation Bias? *Viruses* **2019**, *11*, 596. [[CrossRef](#)]
37. Kim, S.Y.; Jin, W.; Sood, A.; Montgomery, D.W.; Grant, O.C.; Fuster, M.M.; Fu, L.; Dordick, J.S.; Woods, R.J.; Zhang, F.; et al. Characterization of Heparin and Severe Acute Respiratory Syndrome-Related Coronavirus 2 (SARS-CoV-2) Spike Glycoprotein Binding Interactions. *Antivir. Res.* **2020**, *181*, 104873. [[CrossRef](#)]
38. Buchrieser, J.; Dufloo, J.; Hubert, M.; Monel, B.; Planas, D.; Rajah, M.M.; Planchais, C.; Porrot, F.; Guivel-Benhassine, F.; Van der Werf, S.; et al. Syncytia Formation by SARS-CoV-2-Infected Cells. *EMBO J.* **2020**, *39*, e106267. [[CrossRef](#)]
39. Chaudhry, M.Z.; Eschke, K.; Hoffmann, M.; Grashoff, M.; Abassi, L.; Kim, Y.; Brunotte, L.; Ludwig, S.; Kröger, A.; Klawonn, F.; et al. Rapid SARS-CoV-2 Adaptation to Available Cellular Proteases. *J. Virol.* **2022**, *96*, e0218621. [[CrossRef](#)]
40. Nagy, A.; Basiouni, S.; Parvin, R.; Hafez, H.M.; Shehata, A.A. Evolutionary Insights into the Furin Cleavage Sites of SARS-CoV-2 Variants from Humans and Animals. *Arch. Virol.* **2021**, *166*, 2541–2549. [[CrossRef](#)]
41. Liu, Z.; Zheng, H.; Lin, H.; Li, M.; Yuan, R.; Peng, J.; Xiong, Q.; Sun, J.; Li, B.; Wu, J.; et al. Identification of Common Deletions in the Spike Protein of Severe Acute Respiratory Syndrome Coronavirus 2. *J. Virol.* **2020**, *94*, e00790-20. [[CrossRef](#)]
42. Anand, P.; Puranik, A.; Aravamudan, M.; Venkatakrishnan, A.J.; Soundararajan, V. SARS-CoV-2 Strategically Mimics Proteolytic Activation of Human ENaC. *eLife* **2020**, *9*, e58603. [[CrossRef](#)]
43. Dahms, S.O.; Hardes, K.; Steinmetzer, T.; Than, M.E. X-Ray Structures of the Proprotein Convertase Furin Bound with Substrate Analogue Inhibitors Reveal Substrate Specificity Determinants beyond the S4 Pocket. *Biochemistry* **2018**, *57*, 925–934. [[CrossRef](#)]
44. Tian, S.; Huajun, W.; Wu, J. Computational Prediction of Furin Cleavage Sites by a Hybrid Method and Understanding Mechanism Underlying Diseases. *Sci. Rep.* **2012**, *2*, 261. [[CrossRef](#)]
45. Shiryaev, S.A.; Chernov, A.V.; Golubkov, V.S.; Thomsen, E.R.; Chudin, E.; Chee, M.S.; Kozlov, I.A.; Strongin, A.Y.; Cieplak, P. High-Resolution Analysis and Functional Mapping of Cleavage Sites and Substrate Proteins of Furin in the Human Proteome. *PLoS ONE* **2013**, *8*, e54290. [[CrossRef](#)]
46. Örd, M.; Faustova, I.; Loog, M. The Sequence at Spike S1/S2 Site Enables Cleavage by Furin and Phospho-Regulation in SARS-CoV2 but Not in SARS-CoV1 or MERS-CoV. *Sci. Rep.* **2020**, *10*, 16944. [[CrossRef](#)] [[PubMed](#)]
47. Carabelli, A.M.; Peacock, T.P.; Thorne, L.G.; Harvey, W.T.; Hughes, J.; de Silva, T.I.; Peacock, S.J.; Barclay, W.S.; de Silva, T.I.; Towers, G.J.; et al. SARS-CoV-2 Variant Biology: Immune Escape, Transmission and Fitness. *Nat. Rev. Microbiol.* **2023**, *21*, 162–177. [[CrossRef](#)] [[PubMed](#)]
48. Gangavarapu, K.; Latif, A.A.; Mullen, J.L.; Alkuzweny, M.; Hufbauer, E.; Tsueng, G.; Haag, E.; Zeller, M.; Aceves, C.M.; Zaiets, K.; et al. Outbreak.Info Genomic Reports: Scalable and Dynamic Surveillance of SARS-CoV-2 Variants and Mutations. *medRxiv* **2022**. [[CrossRef](#)]
49. Lan, J.; Ge, J.; Yu, J.; Shan, S.; Zhou, H.; Fan, S.; Zhang, Q.; Shi, X.; Wang, Q.; Zhang, L.; et al. Structure of the SARS-CoV-2 Spike Receptor-Binding Domain Bound to the ACE2 Receptor. *Nature* **2020**, *581*, 215–220. [[CrossRef](#)] [[PubMed](#)]
50. Molloy, S.S.; Bresnahan, P.A.; Leppla, S.H.; Klimpel, K.R.; Thomas, G. Human Furin Is a Calcium-Dependent Serine Endoprotease That Recognizes the Sequence Arg-X-X-Arg and Efficiently Cleaves Anthrax Toxin Protective Antigen. *J. Biol. Chem.* **1992**, *267*, 16396–16402. [[CrossRef](#)] [[PubMed](#)]
51. Thomas, G. Furin at the Cutting Edge: From Protein Traffic to Embryogenesis and Disease. *Nat. Rev. Mol. Cell Biol.* **2002**, *3*, 753–766. [[CrossRef](#)]
52. Ginefra, P.; Filippi, B.G.H.; Donovan, P.; Bessonard, S.; Constam, D.B. Compartment-Specific Biosensors Reveal a Complementary Subcellular Distribution of Bioactive Furin and PC7. *Cell Rep.* **2018**, *22*, 2176–2189. [[CrossRef](#)]
53. Casey, J.R.; Grinstein, S.; Orłowski, J. Sensors and Regulators of Intracellular PH. *Nat. Rev. Mol. Cell Biol.* **2010**, *11*, 50–61. [[CrossRef](#)]
54. Stieneke-Gröber, A.; Vey, M.; Angliker, H.; Shaw, E.; Thomas, G.; Roberts, C.; Klenk, H.D.; Garten, W. Influenza Virus Hemagglutinin with Multibasic Cleavage Site Is Activated by Furin, a Subtilisin-like Endoprotease. *EMBO J.* **1992**, *11*, 2407–2414. [[CrossRef](#)]
55. Bolt, G.; Pedersen, L.Ø.; Birkeslund, H.H. Cleavage of the Respiratory Syncytial Virus Fusion Protein Is Required for Its Surface Expression: Role of Furin. *Virus Res.* **2000**, *68*, 25–33. [[CrossRef](#)] [[PubMed](#)]
56. Hallenberger, S.; Bosch, V.; Angliker, H.; Shaw, E.; Klenk, H.-D.; Garten, W. Inhibition of Furin-Mediated Cleavage Activation of HIV-1 Glycoprotein Gp160. *Nature* **1992**, *360*, 358–361. [[CrossRef](#)] [[PubMed](#)]
57. Volchkov, V.E.; Feldmann, H.; Volchkova, V.A.; Klenk, H.-D. Processing of the Ebola Virus Glycoprotein by the Proprotein Convertase Furin. *Proc. Natl. Acad. Sci. USA* **1998**, *95*, 5762. [[CrossRef](#)]
58. Pasquato, A.; Dettin, M.; Basak, A.; Gambaretto, R.; Tonin, L.; Seidah, N.G.; Di Bello, C. Heparin Enhances the Furin Cleavage of HIV-1 Gp160 Peptides. *FEBS Lett.* **2007**, *581*, 5807–5813. [[CrossRef](#)] [[PubMed](#)]

59. Preliminary Genomic Characterisation of an Emergent SARS-CoV-2 Lineage in the UK Defined by a Novel Set of Spike Mutations-NCov-2019 Genomic Epidemiology-Virological. Available online: <https://virological.org/t/preliminary-genomic-characterisation-of-an-emergent-sars-cov-2-lineage-in-the-uk-defined-by-a-novel-set-of-spike-mutations/563> (accessed on 14 September 2022).
60. Volz, E.; Mishra, S.; Chand, M.; Barrett, J.C.; Johnson, R.; Geidelberg, L.; Hinsley, W.R.; Laydon, D.J.; Dabrera, G.; O'Toole, Á. Assessing Transmissibility of SARS-CoV-2 Lineage B.1.1.7 in England. *Nature* **2021**, *593*, 266–269. [[CrossRef](#)] [[PubMed](#)]
61. Mohammad, A.; Abubaker, J.; Al-Mulla, F. Structural Modelling of SARS-CoV-2 Alpha Variant (B.1.1.7) Suggests Enhanced Furin Binding and Infectivity. *Virus Res.* **2021**, *303*, 198522. [[CrossRef](#)] [[PubMed](#)]
62. Liu, Y.; Liu, J.; Johnson, B.A.; Xia, H.; Ku, Z.; Schindewolf, C.; Widen, S.G.; An, Z.; Weaver, S.C.; Menachery, V.D.; et al. Delta Spike P681R Mutation Enhances SARS-CoV-2 Fitness over Alpha Variant. *Cell Rep.* **2022**, *39*, 110829. [[CrossRef](#)]
63. Arora, P.; Sidarovich, A.; Graichen, L.; Hörnich, B.; Hahn, A.; Hoffmann, M.; Pöhlmann, S. Functional Analysis of Polymorphisms at the S1/S2 Site of SARS-CoV-2 Spike Protein. *PLoS ONE* **2022**, *17*, e0265453. [[CrossRef](#)]
64. Lubinski, B.; Fernandes, M.H.V.; Frazier, L.; Tang, T.; Daniel, S.; Diel, D.G.; Jaimes, J.A.; Whittaker, G.R. Functional Evaluation of the P681H Mutation on the Proteolytic Activation of the SARS-CoV-2 Variant B.1.1.7 (Alpha) Spike. *iScience* **2022**, *25*, 103589. [[CrossRef](#)] [[PubMed](#)]
65. Bertelli, A.; D'Ursi, P.; Campisi, G.; Messali, S.; Milanese, M.; Giovanetti, M.; Ciccozzi, M.; Caccuri, F.; Caruso, A. Role of Q675H Mutation in Improving SARS-CoV-2 Spike Interaction with the Furin Binding Pocket. *Viruses* **2021**, *13*, 2511. [[CrossRef](#)]
66. Hodcroft, E.B.; Domman, D.B.; Snyder, D.J.; Oguntuyo, K.Y.; Van Diest, M.; Densmore, K.H.; Schwalm, K.C.; Femling, J.; Carroll, J.L.; Scott, R.S.; et al. Emergence in Late 2020 of Multiple Lineages of SARS-CoV-2 Spike Protein Variants Affecting Amino Acid Position 677. *medRxiv* **2021**. [[CrossRef](#)]
67. Grabowski, F.; Preibisch, G.; Giziński, S.; Kochańczyk, M.; Lipniacki, T. SARS-CoV-2 Variant of Concern 202012/01 Has about Twofold Replicative Advantage and Acquires Concerning Mutations. *Viruses* **2021**, *13*, 392. [[CrossRef](#)]
68. Jung, C.; Kmiec, D.; Koepke, L.; Zech, F.; Jacob, T.; Sparrer, K.M.J.; Kirchhoff, F. Omicron: What Makes the Latest SARS-CoV-2 Variant of Concern So Concerning? *J. Virol.* **2022**, *96*, e02077-21. [[CrossRef](#)] [[PubMed](#)]
69. Yamasoba, D.; Kimura, I.; Nasser, H.; Morioka, Y.; Nao, N.; Ito, J.; Uriu, K.; Tsuda, M.; Zahradnik, J.; Shirakawa, K.; et al. Virological Characteristics of SARS-CoV-2 BA.2 Variant. *bioRxiv* **2022**. [[CrossRef](#)]
70. Lubinski, B.; Jaimes, J.A.; Whittaker, G.R. Intrinsic Furin-Mediated Cleavability of the Spike S1/S2 Site from SARS-CoV-2 Variant B.1.529 (Omicron). *bioRxiv* **2022**. [[CrossRef](#)]
71. Singh, J.; Rahman, S.A.; Ehtesham, N.Z.; Hira, S.; Hasnain, S.E. SARS-CoV-2 Variants of Concern Are Emerging in India. *Nat. Med.* **2021**, *27*, 1131–1133. [[CrossRef](#)]
72. Lubinski, B.; Frazier, L.E.; Phan, M.V.T.; Bugembe, D.L.; Cunningham, J.L.; Tang, T.; Daniel, S.; Cotten, M.; Jaimes, J.A.; Whittaker, G.R. Spike Protein Cleavage-Activation in the Context of the SARS-CoV-2 P681R Mutation: An Analysis from Its First Appearance in Lineage A.23.1 Identified in Uganda. *Microbiol. Spectr.* **2022**, *10*, e01514-22. [[CrossRef](#)]
73. Zhang, L.; Mann, M.; Syed, Z.; Reynolds, H.M.; Tian, E.; Samara, N.L.; Zeldin, D.C.; Tabak, L.A.; Ten Hagen, K.G. Furin Cleavage of the SARS-CoV-2 Spike Is Modulated by O-Glycosylation. *bioRxiv* **2021**. [[CrossRef](#)] [[PubMed](#)]
74. Dahms, S.O.; Creemers, J.W.M.; Schaub, Y.; Bourenkov, G.P.; Zögg, T.; Brandstetter, H.; Than, M.E. The Structure of a Furin-Antibody Complex Explains Non-Competitive Inhibition by Steric Exclusion of Substrate Conformers. *Sci. Rep.* **2016**, *6*, 34303. [[CrossRef](#)] [[PubMed](#)]
75. Henrich, S.; Cameron, A.; Bourenkov, G.P.; Kiefersauer, R.; Huber, R.; Lindberg, I.; Bode, W.; Than, M.E. The Crystal Structure of the Proprotein Processing Proteinase Furin Explains Its Stringent Specificity. *Nat. Struct. Mol. Biol.* **2003**, *10*, 520–526. [[CrossRef](#)] [[PubMed](#)]
76. Long, S.W.; Olsen, R.J.; Christensen, P.A.; Bernard, D.W.; Davis, J.J.; Shukla, M.; Nguyen, M.; Saavedra, M.O.; Yerramilli, P.; Pruitt, L.; et al. Molecular Architecture of Early Dissemination and Massive Second Wave of the SARS-CoV-2 Virus in a Major Metropolitan Area. *mBio* **2020**, *11*, e02707-20. [[CrossRef](#)] [[PubMed](#)]
77. Venyaminov, S.Y.; Baikarov, I.A.; Shen, Z.M.; Wu, C.S.C.; Yang, J.T. Circular Dichroic Analysis of Denatured Proteins: Inclusion of Denatured Proteins in the Reference Set. *Anal. Biochem.* **1993**, *214*, 17–24. [[CrossRef](#)] [[PubMed](#)]
78. Greenfield, N.J. Using Circular Dichroism Spectra to Estimate Protein Secondary Structure. *Nat. Protoc.* **2006**, *1*, 2876–2890. [[CrossRef](#)] [[PubMed](#)]
79. Jackson, M.; Mantsch, H.H. The Use and Misuse of FTIR Spectroscopy in the Determination of Protein Structure. *Crit. Rev. Biochem. Mol. Biol.* **1995**, *30*, 95–120. [[CrossRef](#)]
80. Jackson, C.B.; Farzan, M.; Chen, B.; Choe, H. Mechanisms of SARS-CoV-2 Entry into Cells. *Nat. Rev. Mol. Cell Biol.* **2022**, *23*, 3–20. [[CrossRef](#)]
81. Rabaan, A.; Al-Ahmed, S.; Haque, S.; Sah, R.; Tiwari, R.; Malik, Y.S.; Dhama, K.; Yattoo, I.; Bonilla-Aldana, K.; Rodriguez-Morales, A. SARS-CoV-2, SARS-CoV, and MERS-COV: A Comparative Overview. *Infez. Med.* **2020**, *28*, 174–184.
82. Neumann, G.; Geisbert, T.W.; Ebihara, H.; Geisbert, J.B.; Daddario-DiCaprio, K.M.; Feldmann, H.; Kawaoka, Y. Proteolytic Processing of the Ebola Virus Glycoprotein Is Not Critical for Ebola Virus Replication in Nonhuman Primates. *J. Virol.* **2007**, *81*, 2995–2998. [[CrossRef](#)] [[PubMed](#)]
83. Dahms, S.O.; Hades, K.; Becker, G.L.; Steinmetzer, T.; Brandstetter, H.; Than, M.E. X-Ray Structures of Human Furin in Complex with Competitive Inhibitors. *ACS Chem. Biol.* **2014**, *9*, 1113–1118. [[CrossRef](#)] [[PubMed](#)]

84. Kadam, S.B.; Sukhramani, G.S.; Bishnoi, P.; Pable, A.A.; Barvkar, V.T. SARS-CoV-2, the Pandemic Coronavirus: Molecular and Structural Insights. *J. Basic Microbiol.* **2021**, *61*, 180–202. [[CrossRef](#)] [[PubMed](#)]
85. Decroly, E.; Wouters, S.; Di Bello, C.; Lazure, C.; Ruysschaert, J.-M.; Seidah, N.G. Identification of the Paired Basic Convertases Implicated in HIV Gp160 Processing Based on in Vitro Assays and Expression in CD4+ Cell Lines\*. *J. Biol. Chem.* **1996**, *271*, 30442–30450. [[CrossRef](#)]

**Disclaimer/Publisher's Note:** The statements, opinions and data contained in all publications are solely those of the individual author(s) and contributor(s) and not of MDPI and/or the editor(s). MDPI and/or the editor(s) disclaim responsibility for any injury to people or property resulting from any ideas, methods, instructions or products referred to in the content.